

Physics Opportunities with a TeV Linear Collider

Sally Dawson^a, Mark Oreglia^b

^a Brookhaven National Laboratory, Upton, NY 11973

^b The Enrico Fermi Institute, Chicago, IL 60637

KEYWORDS: linear collider, electron-positron annihilation, Higgs, SUSY

ABSTRACT:

We discuss the physics motivations for building a 500 GeV–1 TeV electron-positron linear collider. The state of the art collider technologies and the physics-driven machine parameters are discussed. A survey of some of the phenomena well suited to study at a linear collider are described, including Higgs bosons, supersymmetry, other extensions to the Standard Model, and cosmology.

CONTENTS

Introduction	2
<i>The Legacy of LEP and SLC</i>	2
<i>New Realities and Possibilities</i>	4
<i>A Roadmap for High Energy Physics</i>	4
<i>Physics-driven Accelerator Requirements</i>	5
<i>Technologies and Issues for a Linear Collider</i>	7
<i>Collision Options</i>	9
<i>Detector Challenges</i>	10
Higgs Bosons	17
<i>Producing the Higgs Boson at a Linear Collider</i>	17
<i>Measuring the Higgs Boson Couplings</i>	18
<i>Measuring the Higgs Boson Quantum Numbers</i>	19
<i>Higgs Spectroscopy in a Supersymmetric Model</i>	20
Supersymmetry	25
<i>sleptons</i>	26

arXiv:hep-ph/0403015v1 1 Mar 2004

<i>Charginos and Neutralinos</i>	28
<i>mSUGRA</i>	29
<i>Gauge Mediated Supersymmetry Breaking</i>	29
<i>Extracting the Underlying SUSY Parameters</i>	30
Other Extensions to the Standard Model	34
<i>Strongly Interacting Electroweak Symmetry Breaking</i>	34
<i>Top Mass measurements</i>	35
<i>Extra Dimensions</i>	35
The Linear Collider and Cosmology	43
<i>The Linear Collider and Astrophysics</i>	43
<i>Dark Matter</i>	43
<i>Baryogenesis</i>	45
<i>Dark Energy</i>	46
Conclusions	51
Acknowledgements	51
Bibliography	51

1 Introduction

1.1 *The Legacy of LEP and SLC*

High Energy Physics currently faces more opportunity than ever to address significant questions about the structure of matter. The 1967 Standard Model (SM) (1) of electroweak unification is consistent with experimental observations to accuracies better than a part in 10^3 , and yet it now raises more questions than it answers. The origin of the symmetry breaking which ultimately unifies electromagnetism with the weak force has still not been found. There are theoretical blemishes in an otherwise elegant mathematical model, such as the theoretical Higgs boson mass being unstable to radiative corrections, requiring a suspicious fine-tuning of Standard Model parameters in order to keep the Higgs boson light (2). And then there is the fact that astrophysical observations suggest an abundance of a new kind of matter. Many are convinced that we are poised for discoveries in the near term which will significantly alter the physics landscape.

The precision measurements of electroweak processes by the Large Electron Positron collider (LEP) and the SLAC Linear Collider (SLC), combined with the Tevatron's discovery of the top quark, have demonstrated to remarkable accuracy that a gauge theory involving a mechanism for spontaneous symmetry breaking (SSB) describes physics nearly correctly at energies up to 200 GeV. The energy scale for continued study of the electroweak sector is fundamentally set by the value of the Fermi coupling constant, namely 300 GeV. The LEP and SLD measurements depart from Standard Model predictions for production cross sections and angular distributions at small but statistically significant levels. These differences are generally consistent with modifications of the gauge boson propagators and decay vertices by a virtual particle or particles having properties similar to those of the Higgs boson in the minimal version of the Standard Model (3). Fits to the combined electroweak data suggest¹ that the mass of this particle is in the ~ 100 -200 GeV region (4,5,6). The particle could be the celebrated Higgs boson or some other object responsible for symmetry breaking and particle masses. The electroweak measurements are partially summarized in figure 1 which shows the LEP Electroweak Working Group (5) compilation of W boson and top quark mass measurements. Superimposed on the figure are the minimal Standard Model predictions for the Higgs boson mass, starting from the 95% confidence level lower limit of 114 GeV on its mass as obtained from direct searches by the four LEP experiments (6). The measurements indicate that the Higgs boson or some similar phenomenon is likely to occur at a mass lower than approximately 200 GeV. If the Higgs boson, or some particle which plays the same role in the theory, does not exist below around 1 TeV, then the self-interactions of gauge bosons become strong and unitarity is violated (7). Hence on very general grounds, some new physics is expected at an energy scale below 1 TeV.

Because of the rather well defined nature of the case for new physics at the near-TeV scale, a strategy has been formulated for High Energy Physics over the next 10–20 years. The Large Hadron Collider (LHC) will address many of the issues (8,9), but has different capabilities for discovering new physics than a linear collider because of the capability of a linear collider for high-precision measurements of masses and missing energy and for polarized scattering. Hence the community (10) plans for a machine to address the precision measurements – a linear electron-positron collider (LC). The case for such a machine has convinced the international community that serious efforts are now needed to research and plan for the LC. Studies for a linear electron-positron collider have existed for nearly 20 years, an excellent review of LC physics appeared in this journal 9 years ago (11), and there are a number of LC physics reviews (12,18,13,14,15,16,17) ... so what can we add to the case now? The answer is: better understanding and new theoretical possibilities. The legacy of LEP and SLC's precision mapping of the electroweak terrain, coupled with the recent and exciting discoveries in astrophysics, have led to extensions to the Standard Model and completely new theories for which we need to again explore the suitability of the High Energy Physics tools of the coming years. Additionally, there have been significant advances in the

¹The limit on the Higgs mass from fits to precision electroweak data is very dependent on the top quark mass; an increase in the top mass by ~ 30 GeV increases the bound on the Higgs to roughly 280 GeV. These fits also assume the validity of the minimal Standard Model with a single Higgs boson. The inclusion of new physics at the TeV scale can significantly change this bound.

LC technology, which we attempt to summarize here.

1.2 New Realities and Possibilities

There are now several theoretical alternatives to the Standard Model Higgs boson, all of them aiming to cure the blemishes of the minimal model. Perhaps the Higgs excitation is a fermion “Cooper pair” achieved by introducing a new set of strong interactions at the TeV scale (19,20). In the “Little Higgs” theory, the Higgs boson is a composite Nambu-Goldstone boson similar to the pion (21). New, heavy gauge bosons might exist which could help with the fine tuning by means of loop corrections. Perhaps there is no Higgs boson at all; divergences could be cancelled by introducing an infinite tower of new particles in extra dimensions (22).

Astrophysical measurements convincingly show that approximately 80% of the matter in the universe is non-baryonic and that there is an astonishingly large amount of dark energy (23). While the dark energy issue continues to be baffling, the dark matter could well consist of as yet undiscovered particles proposed to address some of the Standard Model deficiencies. The nature of the dark matter suggests that it interacts weakly; theoretical models such as supersymmetry (SUSY) would furnish good candidates for the dark matter (24, 25). The existence of supersymmetric particles would also offer a solution to the Standard Model’s fine-tuning problem. Here there is also the exciting possibility that a precision electroweak machine could be a window on Planck-scale physics (e.g., if gravity mediates the supersymmetry breaking).

String theory now offers the possibility that there are more than three spatial dimensions, and that there might be new particle excitations related to the space-time structure. A low-background precision energy e^+e^- linear collider would see a distinct spectrum of narrow mass states arising from excitations of the spatial structures (26).

The possibilities mentioned above are just a few of the new ideas emerging to try to reconcile the Standard Model with Planck-scale physics. While the theories are becoming numerous, they all have the likelihood of new discoveries at the proposed LC energy. The complex nature of many of the new theories will require a low-background, precision energy collider to fully reveal the theoretical structure.

1.3 A Roadmap for High Energy Physics

Currently, the Fermilab Tevatron is taking data on proton-antiproton collisions at a center-of-mass energy of nearly 2 TeV. While this energy is in the range of some possible new phenomena, the backgrounds and luminosity of the collider make it difficult to observe production of particles with Higgs boson rates. Experiments at this machine have a better chance to discover larger cross section processes such as supersymmetric particles. Tevatron data taking is expected to continue for the remainder of this decade.

CERN's LHC is expected to be commissioned in 2007. This machine collides protons at a center of mass energy of 14 TeV. The energy and luminosity are well matched for good identification of the Higgs boson and many candidate particles occurring in extensions to the Standard Model; in particular, a SM Higgs boson could be identified in 1 or 2-years of running for any mass within the reasonable range of the theory (9). However, since the center-of-mass energy of the fundamental collision is not known, and the beams are not polarized, a number of high precision measurements cannot be made. The LHC will likely produce the particles responsible for symmetry breaking, but it will give us only partial knowledge of their qualities.

The LC designs under consideration address precisely the limitations of the LHC, though at a lower mass reach. But, more importantly, the LC capability of low-background precision measurements opens a window to new physics. In the best of worlds, LHC and LC data-taking would overlap so that the two facilities could engage in feedback which would strengthen our knowledge of nature. The case for combined running and complementarity between the LHC and a LC has been the topic of intense study (27). An example of what is gained this way is realized by the complex chain of the decay of supersymmetric particles. If supersymmetric particles exist, and they play the expected role in curing the hierarchy problem, the LHC is likely to produce many of them. Sleptons, in particular, are difficult to identify cleanly at the LHC because they are produced with a small rate and large background with missing energy in the decay. The LC could provide these particle masses with much higher precision than the LHC, and there are scenarios in which the LHC would not detect these sparticles at all; in such cases the mass information from the linear collider would strengthen the LHC probe of the supersymmetric parameter space at the highest energies (28). In addition, the capability of a linear collider to make precise measurements of the couplings of new particles will be crucial in order to verify that the new particles correspond to an underlying supersymmetric model. Some concurrent running of the two facilities suggests an LC construction schedule. LHC startup is expected in 2007, with real physics output expected throughout 2008-2020. Consequently, it would be desirable to have the LC operational in 2015-17. This would imply initiation of LC construction by the end of this decade. A construction start at that time would be informed by the first LHC results.

1.4 *Physics-driven Accelerator Requirements*

The performance criteria enabling a LC to achieve the desired physics measurements have recently been stated by the American Linear Collider Physics Group (ALCPG) (29) and (with nearly identical conclusions) by a committee established by the International Linear Collider Steering Group (30). The major issues concern the energy, luminosity, and beam qualities.

It is reasonable to assume that the initial LC physics program would have as its top goal copious production of the lowest mass Higgs boson(s) or other particles in the 115-200 GeV mass range indicated by LEP and SLD precision measurements (4,5,6). The Standard Model production rates for the Higgs boson are lower than those for most popular alternative physics scenarios, so it is this Standard Model rate that sets the luminosity requirement for the machine. Even if the current

electroweak precision measurements suggest a Higgs boson mass no higher than approximately 200 GeV, the machine energy must be higher than this mass for two reasons. Firstly, the important ‘‘Higgstrahlung’’ production mechanism (section 2.1) $e^+e^- \rightarrow Zh$ has a maximum yield for a center-of-mass energy $\sqrt{s} = 220 - 340$ GeV for Higgs masses in the 115 – 200 GeV range. Second, detailed understanding of the particle properties will require measuring the Higgs self-coupling, the hW^+W^- coupling, and (for a higher mass Higgs) the decay $h \rightarrow t\bar{t}$ (31,32). These processes suggest a baseline machine energy of 500 GeV, with the capability to tune the energy in order to perform threshold scans and some running at the Z peak.

The machine luminosity should be capable of producing enough Higgs bosons to measure cross sections and couplings at the 5% level in order to distinguish among the models (15, 34, 33) proposed to extend the Standard Model. The maximum Standard Model Higgs production cross sections (in association with a Z boson) vary from about 300 fb at $M_h = 115$ GeV to about 70 fb at $M_h = 200$ GeV. Assuming that the luminosity scales linearly with \sqrt{s} , the higher end of the mass range dictates the LC luminosity requirements, namely an integrated luminosity of 500 fb^{-1} .

Because precision electroweak measurements and astrophysical arguments strongly indicate new physics in the energy range of 100 GeV to beyond 1 TeV, the linear collider will need to be upgraded to the TeV energy range after the initial physics period. Exploration of the TeV energy region will be crucial for our understanding of the Standard Model and for addressing the indirect evidence of new physics. The best place to study rare or low-rate Higgs decays is at higher energy using W^+W^- fusion, $e^+e^- \rightarrow h\nu\bar{\nu}$ (section 2.1 and reference (35)). This process has a cross section which increases with energy. Running at an energy near 1 TeV will allow for good determination of small branching fractions such as $h \rightarrow \mu^+\mu^-$ (36) with a fraction of the integrated luminosity it would take using the $e^+e^- \rightarrow Zh$ process at $\sqrt{s} = 500$ GeV. For light Higgs bosons, an important channel to measure is radiation of a Higgs boson by a top quark in $e^+e^- \rightarrow t\bar{t}h$ (section 2.2 and reference (15)). Other new physics processes benefit from the highest energy reach, even at reduced luminosity. For example, limits obtained on fermion compositeness and extra gauge bosons from the reaction $e^+e^- \rightarrow f\bar{f}$ scale as $(s^2L)^{0.25}$; for graviton exchange, the limits scale as $(s^3L)^{0.125}$ (15), where L is the total integrated luminosity. In strong symmetry breaking scenarios one will want to study final states with W^+W^- , ZZ , and $t\bar{t}$, which is most effectively done at the TeV energy scale.

The LC will need to produce polarized beams in order to exploit the parity violation intrinsic to the electroweak model and to identify the quantum numbers of new particles. An added bonus of polarized beams is the enhancement of signal reactions compared to most backgrounds. Currently it is feasible to polarize the electron beam to better than 80% as established by SLC, but positron polarization remains at the research and development stage. Even if the machine were to operate with only polarized electrons, much better sensitivity to SM parameters in W^+W^- and $t\bar{t}$ production would be observed (section 4.2), and it would allow for selection of specific chirality in supersymmetric particle production (section 3). Electron polarization of 80% or more is very effective in identifying selectrons in supersymmetric theories, where each lepton has two scalar partners

which are produced preferentially from polarized electron beams of opposite polarization.

Positron polarization increases the effective polarization, defined as

$$P_{eff} \equiv \frac{|P_-| + |P_+|}{1 + |P_- P_+|}, \quad (1)$$

where P_+ , P_- are the electron and positron polarizations. This results in higher production rates of a number of physics processes, including Zhh and W^+W^-hh production (37). Annihilation through a photon or virtual Z takes place from the polarization states $e_L^- e_R^+$ and $e_R^- e_L^+$ only. By polarizing the positron beam opposite to the electron beam, these channels are enhanced and better defined. For 80% electron polarization, the introduction of 60% positron polarization leads to an effective polarization of 95% and an increase in the annihilation rate by a factor 1.5, assuming no loss of intensity as a result of the positron polarization (15). Additionally, positron polarization aids in background suppression. With an e_R^- beam, introduction of a 60% polarized positron beam leads to a further factor of three background suppression of W^+W^- pairs. Positron polarization can also be used to control signal and background reactions involving t -channel exchange. If the selectron appears at the LC, positron polarization can select whether the partner of the e_L^+ or e_R^+ is produced. Single W^+ production is a background for some analyses, and this can also be controlled by using a polarized e_L^+ beam.

1.5 Technologies and Issues for a Linear Collider

1.5.1 Accelerating Structures

Electron storage rings cease to be effective for beam energies much above 100 GeV because the power lost to synchrotron radiation grows as E_{beam}^4 . The total cost of electron synchrotrons scales roughly as E_{beam}^2 , whereas the scaling is linear for linear accelerating structures (38). The only practical alternative for a next-generation electron accelerator is to collide bunches accelerated in linear structures. For cost reasons these linacs need to employ higher acceleration gradients than used previously, and this is facilitated by going to higher RF frequencies. The luminosity scales as (beam power)/(beam area), with cost optimization requiring nanometer-scale beam area. Three acceleration methods have been under development for well over a decade, two of which look very promising for implementation in the short term (39).

- Superconducting (or “cold”) RF cavities are the main feature of the TESLA (16) proposal. With superconducting structures, surface power density must be limited and cryogenic losses increase as ω^2 (where ω is the RF frequency), so relatively long RF wavelength (1.4 GHz, or L-band) must be employed. Accelerating structures capable of 35 MV/m have been constructed and tested. This technology requires a relatively long time between pulses because of the high-Q cavities. The TESLA layout is shown in figure 2 (16).

- Normal conducting (or “warm”) RF cavities (40,41) have recently been developed with beam-loaded gradients of 50 MV/m. In these structures stored energy scales as ω^{-2} and surface breakdown resistance as ω , so it is desirable to use the highest RF frequency possible. The higher X-band (11.4 GHz) frequency would be most cost effective; a C-band (5.7 GHz) version is also under consideration. Like the superconducting case, the warm RF structures would be driven by conventional klystrons. However, the warm RF scheme puts much greater stress on the klystrons, requiring higher efficiency and much higher peak power. The warm RF layout of the “NLC” scheme is shown in figure 3 (40).
- The use of klystrons in L, C, and X band technologies is practical for beam energies up to approximately 1 TeV, beyond which the power costs become prohibitive. To reach the 3 TeV range, the Compact Linear Collider (CLIC) (42) group derives the RF power from deceleration of a high-current, low-energy bunched beam. It is thought that higher surface damage thresholds can be achieved by using yet higher RF frequencies, so CLIC is developing 30 GHz RF structures. This technology could conceivably achieve gradients of 150 MV/m. Research and development of this challenging technology is underway, but it is not expected to be demonstrated in the near term.

At the time this article was written, several issues with both the warm and cold technology were identified by the Technical Review Committee of the International Linear Collider Steering Committee (43). To grossly summarize the main issues raised in their exhaustive study, it appears that both technologies are feasible. The two areas most urgently identified for more study are RF damage in the warm cavities and the feasibility of large-scale production of cryogenic RF modules capable of 35 MV/m with acceptable quenching and breakdown rates. In addition, the extremely long damping rings needed by the cold technology raise some concern. The choice of a technology will be made by the International LC Steering Committee (ILCSC) after considering the recommendations of its Technical Recommendation Panel (44).

1.5.2 Beam Structure

The superconducting and warm RF structures require markedly different bunch structures. The long time constants associated with superconducting cavities lead to 950 μ s pulses at a 5 Hz repetition rate, while the warm RF has 267 ns pulses repeated at 120 Hz or 150 Hz. The time between bunches in each pulse is 337 ns for superconducting RF and 1.4 ns for warm RF. The detector design must accommodate these differences in beam structure. The long interbunch period for cold RF allows detectors to read and clear between collisions, but the overall pulse structure does not allow for easy electronics power cycling to minimize cooling systems. The warm RF time structure does accommodate power cycling, but most detector electronics will not be able to read individual bunch crossings, so there will be pileup and duty factor issues.

1.5.3 Beam Size and Collision Energy

In order to achieve the luminosity required by the physics, the beams must have nanometer scale transverse dimensions. This requirement introduces special challenges for both the accelerator and the detectors. The small bunch size at the collision point requires that the accelerator maintain tight tolerances on the beam phase space (or “emittance”) through the several stages of transport, and that beam jitter due to ground motion or other noise sources be actively or passively corrected. Several groups have demonstrated the feasibility of active feedback corrections for beam jitter, though more work in this area is needed.

The extreme charge density at the collision point leads to new phenomena – and some problems – for linear colliders, namely beam-beam disruption, luminosity enhancement, photon emission and generation of e^+e^- pairs (38). For oppositely charged colliding beams, the bunches focus each other with a highly nonlinear force. This self-focussing leads to an enhancement in the luminosity by a factor of 1.5 to 2 (40). However, the focussing also results in beams which are more difficult to dispose of and backgrounds in the detector from beam induced synchrotron photons (known colloquially as “beamstrahlung” (45)). The beamstrahlung results in a collision energy spectrum with a very significant low energy tail, as shown in figure 4 (from reference (46)). Unlike the initial state radiation which can be accurately calculated, the luminosity-weighted energy spectrum arises from energy variation in the bunches caused by wake fields in the accelerating structures; the spectrum therefore depends on the machine settings, and this will necessitate new types of beam instrumentation to accurately measure the luminosity spectrum. It is possible that the beams will have to cross at a small angle in the interaction point in order to perform diagnostic measurements of the beams, such as precise measurements of the beam energy, energy spread and polarization. Additionally, instrumentation for measuring the characteristics of the disrupted beam and beamstrahlung may improve the determination of the luminosity-weighted beam energy and polarization. The beam energy spread (~ 1000 ppm rms for TESLA) and luminosity-weighted beamstrahlung energy loss (~ 25000 ppm) are large compared to the desired precision for measuring the top mass, Higgs mass, W mass and the left-right decay product asymmetry (A_{LR}). The luminosity-weighted depolarization may be as large as 0.5% at a 500 GeV LC, while the polarization must be measured with a precision of 0.1-0.25% for the physics program of measuring Standard Model asymmetries. Extraction line polarization measurements may be needed to achieve the desired precision (47). Determining the luminosity-weighted energy and polarization from instrumentation that measures the average energy and polarization is non-trivial, and instrumentation is required which still awaits development (46).

1.6 Collision Options

The LC accelerator can be modified to facilitate e^-e^- , $\gamma\gamma$, and $e^-\gamma$ collisions. The first process, Møller scattering, is the reaction most sensitive to contact interactions and electron compositeness, but there are other situations for which e^-e^- scattering is important to study (48). For example,

selectron pairs can be produced in e^-e^- collisions by t -channel exchange of neutralinos (section 3), with Standard Model backgrounds extremely low. This process offers the best setting for high-precision measurements of the selectron masses and the neutralino masses and mixing angles (49, 50, 51).

The e^-e^- option also affords a low-background method for generating $\gamma\gamma$ and $e^-\gamma$ collisions by scattering a high intensity laser pulse off the electron beams. If the Higgs boson is in the 100-130 GeV mass range, the photon scattering can be used to create a ‘Higgs-factory’ based on s -channel production (15). This facility would permit high precision measurement of the $h \rightarrow \gamma\gamma$ partial width, which is sensitive to new charged particles such as the top squark, and also the top quark Yukawa coupling (52). The effective cross sections for producing Higgs and Supersymmetric particles are as large or even larger than the corresponding ones for e^+e^- , and the capability of this machine to produce linearly polarized beams not only can provide conclusive information about the charge-parity (CP) nature of these particles, but also will allow us to detect any CP admixture (15). Certain rare decays such as $h \rightarrow \gamma\gamma$, $h \rightarrow \gamma Z$, and $h \rightarrow ZZ$ are highly sensitive to parameters of the Minimal Supersymmetric Standard Model (MSSM), and could be cleanly measured with the photon collider. A $\gamma\gamma$ collider could measure the spectrum and CP properties of the heavier Higgs bosons in extended models in $\tan\beta$ and M_A regions that are not accessible to the e^+e^- machine or the LHC. In a high energy e^+e^- mode with unpolarized positrons, the electron beam can be used to produce linearly polarized photons to study the CP nature of the Higgs.

While it will be necessary to occasionally operate the collider at the Z resonance in order to calibrate the detector, one can envision a program of high luminosity running at the ZZ and W^+W^- thresholds in order to perform ultra-high precision measurements of electroweak parameters(54,53). Such a physics program would be worthwhile with approximately 10^8 polarized Z ’s; at this level of statistics, the current uncertainty on the weak mixing angle could be reduced by a factor of 5. If positron polarization is possible, the measurements at the Z resonance would be even more precise.

1.7 Detector Challenges

The detectors used to extract physics from a linear collider face challenges from the accelerator architecture and beam related backgrounds, as well as from the nature of the precision physics measurements needed. Because of the important physics with missing energy signatures, the detector will have to cover as much of the solid angle as possible. The detector will have to incorporate a channel for the disposal of the disrupted beams after collision, and elaborate masking must be devised to minimize the beamstrahlung and other beam backgrounds in the detector, especially near the beampipes. A large background from low energy e^+e^- pairs will require a high magnetic field for the central detector. High-rate two-photon physics processes will create large occupancy at low polar angles (with respect to the beam axis), and therefore a high efficiency low-angle tagger will be needed. The detector issues and emerging designs are summarized in references (55, 56, 57, 58). The physics phenomena driving the detector designs can be summarized as:

- excellent mass resolution (especially from the clean dimuon channel) to measure recoil masses (Higgs bosons), kinematic edges (SUSY spectra), and spectra indicative of other new physics;
- tagging of bottom and charm (Higgs sector, SUSY);
- hadronic energy resolution capable of separating W^\pm from Z jets, as well as Higgs boson and top quark decays (Higgs properties, SUSY, other theories);
- crack-free coverage of the solid angle down to low polar angles for missing energy final states (SUSY, other theories).

The flavor-tagging requires a precision vertex tracker at very small radius. Highly pixellated semiconductor devices are the likely technology for the vertex detector, and new semiconductor technologies promise to reduce the long readout time required by older CCD devices. The physics requires impact parameter resolution of approximately 3-5 μm and a multiple scattering less than $\sim 5\mu\text{m}/p(\text{GeV})$. The vertex detector will also need to be able to survive the large radiation dose near the beampipe.

Particle tracking technologies under consideration include large-volume drift chambers or time projection chambers, and smaller-radius solid-state detectors. It is not yet clear that the necessary precision can be achieved with conventional tracking-detector technologies. The physics requirement on recoil mass resolution requires improvement in the resolution from the current state of the art to $\delta p/p^2 \sim 10^{-5} \text{ GeV}^{-1}$. Because of the large numbers of low energy pairs and multiple collisions during the readout time, pattern recognition for tracking is challenging. High efficiency tracking in the forward regions will be essential for missing energy channels. There is also a potentially significant uncertainty on the dimuon recoil mass measurement from knowledge of the luminosity-weighted energy distribution (15). Since this distribution changes with machine running parameters, instrumentation must be developed which can accurately measure this spectrum.

To discriminate Z decays from W^\pm decays, the calorimeters will need unprecedented jet energy resolution. Figure 5 shows simulations for reconstructed dijet masses for $e^+e^- \rightarrow \nu\bar{\nu} ZZ$ or $e^+e^- \rightarrow \nu\bar{\nu} W^+W^-$. The conclusion drawn is that the jet energy resolution must be $30\%/\sqrt{E(\text{GeV})}$ or better (59). Large diameter hadron calorimeters with the necessary granularity and resolution have never before been built and energy-flow methods for final state reconstruction are still under development. Energy flow techniques benefit from fine granularity in both the electromagnetic and hadronic calorimeters, and with sufficiently small granularity ($\sim 1 \text{ cm}$ pads) it is conceivable that the hadronic calorimeter information can be limited to “digital” mode – that is, each pad is read out as “on” or “off”. It is not entirely clear that separate electromagnetic and hadronic calorimeters, in contrast to a hybrid device, are the optimal choice.

Differences in the bunch-timing structure of warm- and cold RF machines have been mentioned earlier in section 1.5.2. These different time structures will require that detectors be optimized for the machine technology choice from the standpoints of cooling, event pileup, and readout (60). It will be possible to read and clear most detector technologies between cold RF bunches,

but this will likely be impossible for warm RF (but the pileup does not appear to be a problem). The exception to this is the vertex detector. With cold RF, readout can currently be achieved in $50 \mu\text{s}$, which means there will be multiple readouts during the bunch train, and RF noise can be a problem. The warm RF version would read out after the entire bunch train, which avoids the RF noise pickup. With either technology, tracks will need to be time-stamped in order to reduce backgrounds from overlapping collisions, particularly from two-photon processes. The longer inter-bunch spacing in a cold RF machine allows for easier time stamping.

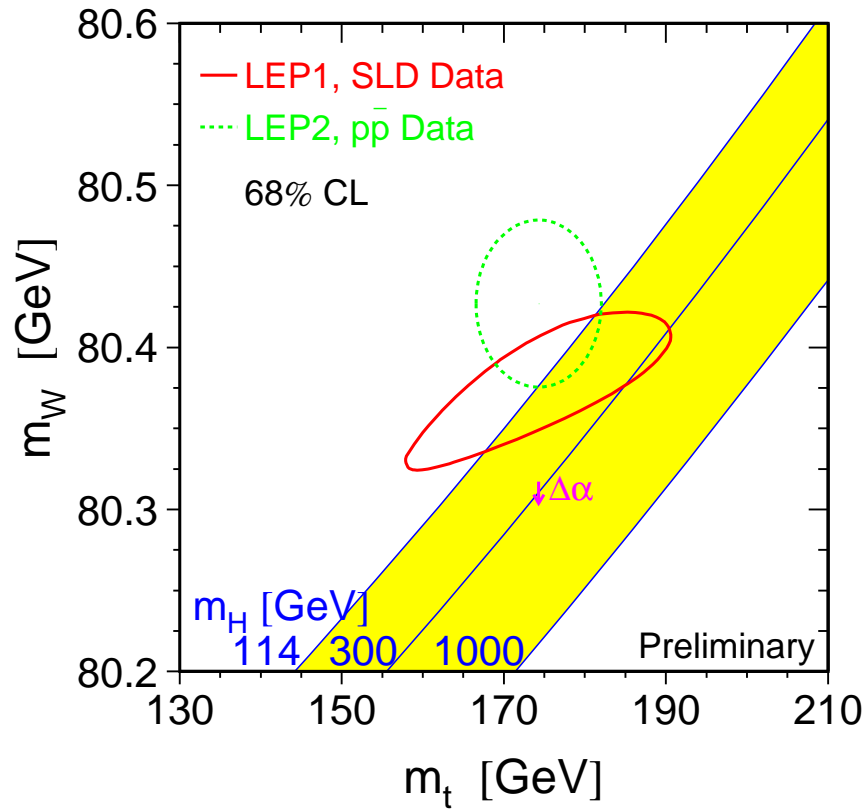
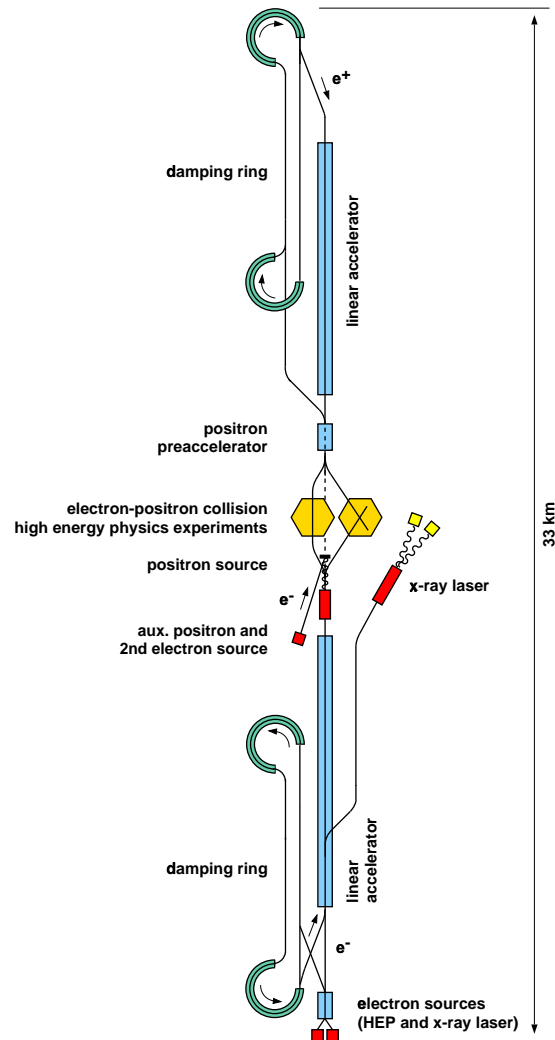


Figure 1: Comparison of the indirect LEP-1 and SLD measurements of the W and top masses (solid contour) and the direct LEP-2 and Tevatron measurements (broken contour). Also shown is the Standard Model relationship for the masses as a function of the Higgs boson mass. The arrow labelled $\Delta\alpha$ shows the variation of this relation if $\alpha(M_Z^2)$ is varied by one standard deviation. From reference (5).



H.Weise 3/2000

Figure 2: *Layout of the preliminary design for the cold RF linear collider TESLA. The horizontal and vertical axes are not to the same scale, so the collision angles appear much larger than they are in reality. From reference (16).*

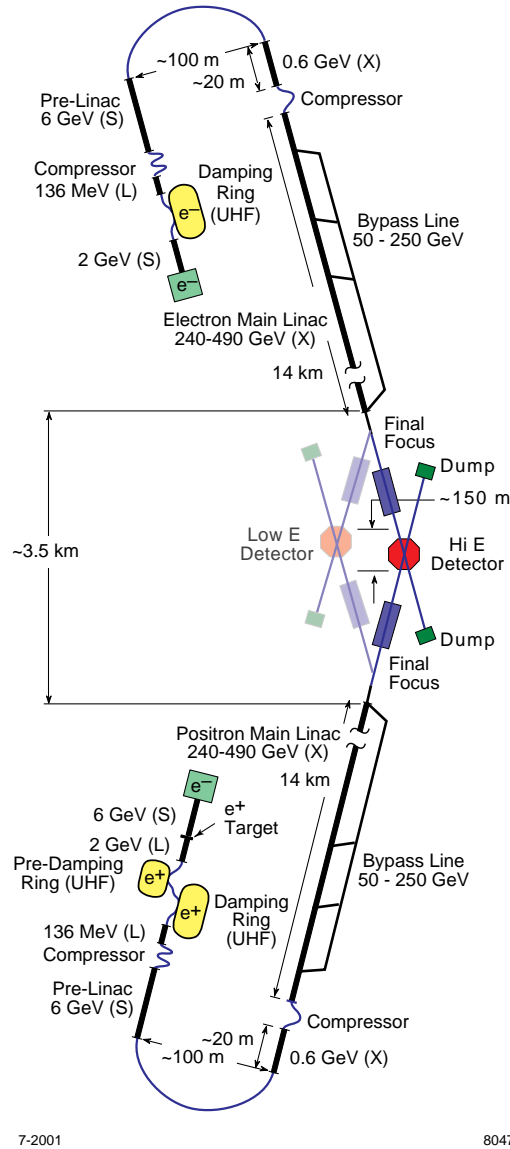


Figure 3: Preliminary design for the warm RF NLC accelerator. The horizontal and vertical axes are not to the same scale, so the collision angles appear much larger than they are in reality. From reference (40).

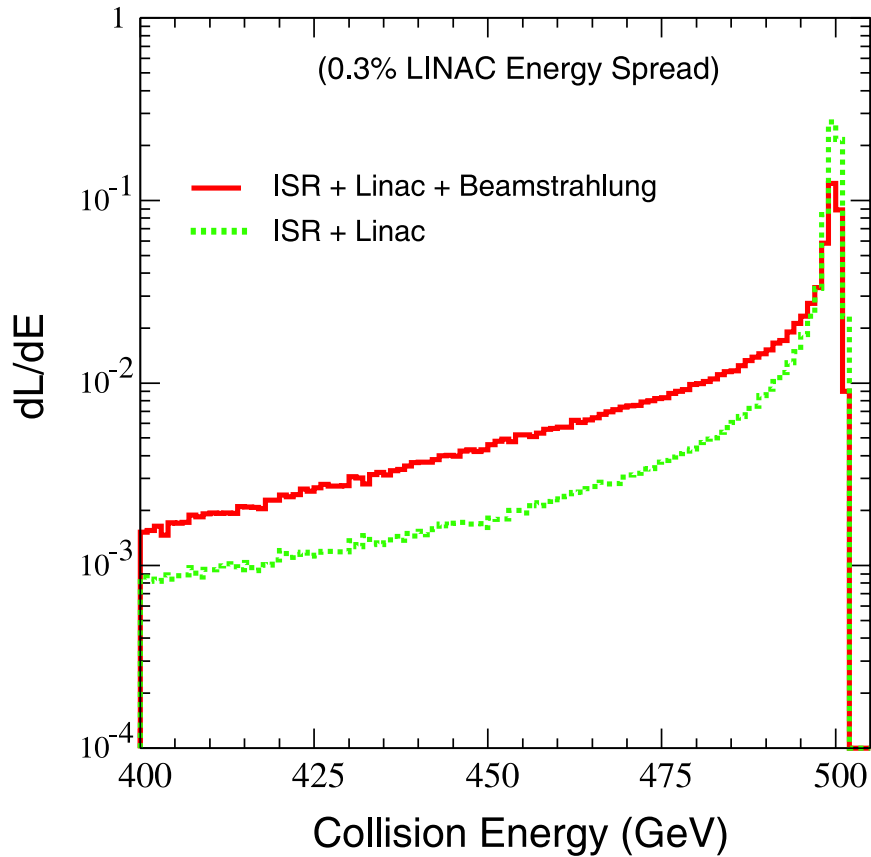


Figure 4: Simulation of the luminosity spectrum expected for a 500 GeV warm RF machine, including the effects of initial state radiation, beamstrahlung, and linac energy spread of 0.3%. From reference (46).

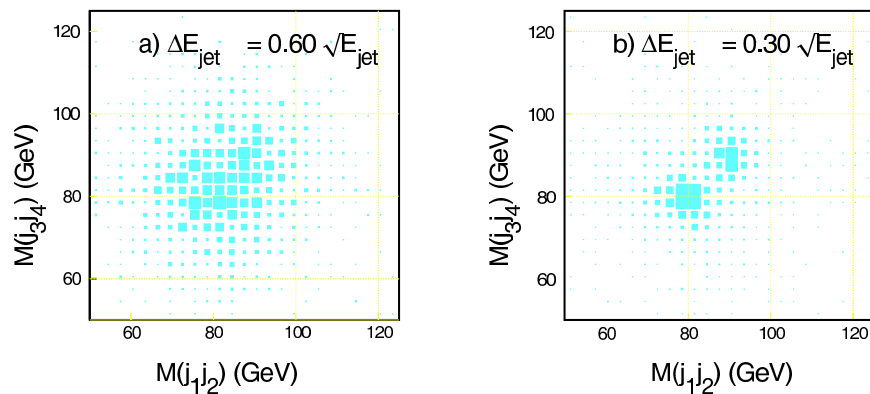


Figure 5: Reconstructed dijet masses from simulation of $e^+e^- \rightarrow \nu\bar{\nu}ZZ$ and $e^+e^- \rightarrow \nu\bar{\nu}WW$. The jet energy resolution in a) is 60%; in b) it is 30%. From reference (59).

2 Higgs Bosons

The experimental successes of the Large Electron Positron (LEP) collider at CERN, the SLAC Linear Collider, and the Tevatron Collider at Fermilab tell us that the standard $SU(2) \times U(1)$ gauge theory describes the interactions of elementary particles at the 200 GeV energy scale to an astounding degree of precision. The model, however, has one glaring flaw: it cannot explain the source of either gauge boson or fermion masses without the existence of an as yet unseen scalar particle. This scalar particle is dubbed the Higgs boson. In the minimal version of the model, all particle masses are proportional to a single parameter, the Higgs vacuum expectation value, v , which is determined by muon decay to be $v = 246$ GeV. The resulting gauge theory has a single unknown quantity, the mass of the Higgs boson, and all observables can be calculated in terms of M_h .

The search for the Higgs boson is one of the most important components of the physics program at both the CERN Large Hadron Collider and a future linear collider. Finding the Higgs boson and measuring its properties will give crucial insight into the underlying origin of mass and help to complete our understanding of the $SU(2) \times U(1)$ gauge theory.

Finding a Higgs boson is only the beginning, however, and inevitably leads to more questions. In order to prove that the Higgs boson is the source of mass and to test the completeness of the minimal Standard Model, three basic sets of measurements are required:

- The couplings of the Higgs boson to fermions and gauge bosons must be proportional to the particle masses. This requires the measurement of Higgs boson branching ratios.
- The Higgs boson must be a spin-0 particle with positive charge and parity.
- The Higgs boson must generate its own mass. This requires measuring the Higgs boson tri-linear and quartic self-couplings.

Should a fundamental Higgs boson not exist, alternative new physics must provide the apparent effects described above (such as particle masses, for example). In section 4, we describe the role of the linear collider in such a scenario.

2.1 Producing the Higgs Boson at a Linear Collider

A Higgs boson can be discovered at the LHC for any value of its mass up to the 1 TeV mass scale (9). However, for most values of the Higgs boson mass, the LHC is sensitive to only a subset of the possible Higgs decays and so is limited in its capability to obtain a complete picture of the Higgs boson couplings to matter (61). A linear collider can expand our knowledge of the Higgs boson properties beyond the LHC capabilities (34).

A linear collider can copiously produce a Higgs boson through both the Higgstrahlung

process,

$$e^+e^- \rightarrow Zh, \quad (2)$$

and the vector boson fusion processes,

$$\begin{aligned} e^+e^- &\rightarrow W^+W^-\nu\bar{\nu} \rightarrow \nu\bar{\nu}h \\ e^+e^- &\rightarrow ZZe^+e^- \rightarrow e^+e^-h. \end{aligned} \quad (3)$$

Both of these production mechanisms are sensitive to the couplings of a Higgs boson to the W and Z gauge bosons.

The Higgstrahlung process reaches its maximum rate at an energy of $\sqrt{s} \sim M_Z + 1.4M_h - 30$ GeV. Measurements of the top quark mass, the W boson mass, and other electroweak precision observables give an indirect limit on the Higgs boson mass of $M_h < 219$ GeV (5), which suggests that the optimal collider energy for observing the Higgs boson through Higgstrahlung is $\sqrt{s} \sim 350 - 500$ GeV. This is one of the major considerations in determining the initial energy scale of a linear collider. On the other hand, the rate for Higgs production through vector boson fusion grows with energy and dominates the production rate at high energy. From figure 6, it is apparent that the dominant production mechanism at high energy is $e^+e^- \rightarrow h\nu\bar{\nu}^2$. The complete set of one-loop electroweak radiative corrections to both Higgstrahlung and vector boson fusion are known, as are the strong $O(\alpha_s)$ corrections (63) and so the predictions are on a firm theoretical basis.

2.2 Measuring the Higgs Boson Couplings

When the Higgs boson is produced in association with a Z boson, missing mass techniques relate the Higgs boson mass to the initial state energy, \sqrt{s} , and the energy of the detected Z boson, E_Z , regardless of how the Higgs boson decays,

$$M_h^2 = s - 2\sqrt{s}E_Z + M_Z^2. \quad (4)$$

Once the total cross section is measured by observing the Z decay products, the various decays of the Higgs boson can be reconstructed and the Higgs couplings to the decay products can be determined unambiguously. There are two techniques for obtaining branching ratios from the $e^+e^- \rightarrow Zh$ process (32). The first is to measure the total cross section for $e^+e^- \rightarrow ZX$ and divide by the $e^+e^- \rightarrow Zh$ cross section obtained from the recoil mass technique. This approach can also obtain the branching ratio for the decay of the Higgs boson into an invisible mode, which occurs in some variants of the Standard Model. The second method is to obtain a sample of hZ events and measure the fraction of events corresponding to $h \rightarrow X$.

The Higgs boson branching ratios are definitive tests of the model (33, 64, 65) and are expected to differ in extensions of the Standard Model (34). For a light Higgs boson, $M_h < 160$ GeV,

²For a heavy Higgs boson, $M_h \gtrsim 500$ GeV, it is important to include the effects of the Higgs boson width. In this case, calculating the on-shell cross section and multiplying by the Higgs boson branching ratio overestimates the rate(62).

the typical precision on the Higgs couplings to fermions ranges from 1 – 3% for the coupling to the b quark, to $\sim 12\%$ for the couplings to the charm quark and the τ lepton (65). The coupling to the muon is expected to be poorly measured, $\sim 30\%$, due to its small magnitude(36).

The top quark is much heavier than the other quarks, $M_t \sim 175$ GeV, and so plays a special role in many extensions of the Standard Model (19). The measurement of the Higgs boson coupling to the top is thus of particular interest. For $M_h < 2M_t$, this coupling is not accessible from Higgs decays, but instead can be measured through the associated production process, $e^+e^- \rightarrow t\bar{t}h$. This mechanism suffers from a small rate and requires high energy, $\sqrt{s} \sim 800 - 1000$ GeV, and high luminosity. An integrated luminosity of $L = 1000 \text{ fb}^{-1}$ is needed for a 10 – 20% measurement of the Higgs-top quark coupling (66).

In the Standard Model, the Higgs boson self-couplings are dictated by the scalar potential,

$$V = \frac{M_h^2}{2}h^2 + \lambda_3vh^3 + \frac{\lambda_4}{4}h^4, \quad (5)$$

where $\lambda_3 = \lambda_4 = \frac{M_h^2}{2v^2}$. Verifying the relationship between λ_3 and λ_4 and the dependence of the self-couplings on the Higgs boson mass is a critical ingredient in demonstrating that the Higgs boson is the source of its own mass. Measuring λ_3 requires the production of two Higgs bosons, and so the rate at both a linear collider and the LHC is very small and requires the highest possible luminosity.

At an energy of $\sqrt{s} = 500$ GeV, an e^+e^- collider is sensitive to the production channel $e^+e^- \rightarrow Zhh$. For $M_h < 140$ GeV, the dominant decay chain is $h \rightarrow b\bar{b}$ and there is a high efficiency for identifying the b's recoiling from the Z boson. This leads to a final state with four b quarks (from the two Higgs boson decays). The tri-linear Higgs self-coupling can be measured to roughly a 20% accuracy for $120 \text{ GeV} < M_h < 140$ GeV with an integrated luminosity of 1000 fb^{-1} in this channel and can definitively exclude $\lambda_3 = 0$ (67,68).

In order to verify the structure of the scalar potential, it is necessary to also measure the Higgs quartic coupling, λ_4 . Unfortunately, this measurement remains elusive at both the LHC and a linear collider because of the smallness of the rate for triple Higgs production(68).

2.3 Measuring the Higgs Boson Quantum Numbers

One of the attractive features of a linear collider is that it can measure the Higgs boson quantum numbers with few assumptions about the underlying model. In order for the Higgs boson to have a vacuum expectation value, and so be the source of mass, it must be a CP (charge/parity) even spin 0 particle. The angular distributions of both the Z and the h in the Higgstrahlung production $e^+e^- \rightarrow Zh$ are sensitive to the spin of the Higgs boson and scale as $d\sigma/d\cos\theta \sim \sin^2\theta$ for a $J^P = 0^+$ particle (69). The spin can also be determined by measuring the dependence of the cross

section on the center-of-mass energy (see figure 7 (70)) and from the invariant mass of the virtual Z boson in the decay, $h \rightarrow ZZ^*$ if $M_h < 2M_Z$ (71). The angular distribution of the decay products in the $h \rightarrow ZZ^*$ decay can also distinguish between a Standard Model Higgs boson and a CP odd, $J^{PC} = 0^{-+}$, pseudoscalar state. These measurements are performed at the hZ threshold energy and demand only a small luminosity, $L \sim 20 \text{ fb}^{-1}$. Determining the Higgs boson quantum numbers from the decay products does not depend on the production mechanism and so can also be used to determine the Higgs spin and charge conjugation in $\gamma\gamma$ collisions. Equivalently, the observation of the decay $h \rightarrow \gamma\gamma$ rules out spin 1 for the Higgs boson.

2.4 Higgs Spectroscopy in a Supersymmetric Model

The model most often used for comparison with the Standard Model is the minimal supersymmetric standard model (MSSM). The MSSM offers a rich phenomenology. In the Higgs boson sector, there are five Higgs bosons: two neutral scalars, h^0 and H^0 , a pseudo-scalar, A^0 , and two charged scalars, H^\pm . Because of the underlying supersymmetry, this is a very predictive model. At the Born level, the Higgs sector has only two free parameters, which are typically taken to be the pseudoscalar mass, M_A , and $\tan\beta$, the ratio of the neutral Higgs boson vacuum expectation values. The lightest Higgs boson has an upper bound somewhere around $M_h < 130 \text{ GeV}$ (72), making it easily observable at an e^+e^- collider with $\sqrt{s} = 500 \text{ GeV}$ through the Higgstrahlung process³.

Precision measurements of the lightest neutral Higgs boson branching ratios can give indirect evidence for the existence of supersymmetry since these rates differ from those of the Standard Model. Quantities such as $R \equiv \Gamma(h^0 \rightarrow b\bar{b})/\Gamma(h^0 \rightarrow \tau\bar{\tau})$ are particularly sensitive to the parameters of the supersymmetric model (74). For large values of $\tan\beta$, this ratio is sensitive to pseudoscalar masses up to 600 GeV, as can be seen in figure 8. A global fit to the expected precision for Higgs boson decay rates at a $\sqrt{s} = 350 \text{ GeV}$ collider with an integrated luminosity of $L = 1000 \text{ fb}^{-1}$ suggests that a linear collider will be able to probe mass scales up to around $M_A \sim 600 \text{ GeV}$ for all values of $\tan\beta$ (75).

As the pseudoscalar mass becomes large, the MSSM approaches a decoupling limit and the Higgs sector looks much like that of the Standard Model. In this limit, A^0 , H^0 and the charged Higgs bosons, H^\pm are almost degenerate in mass and much heavier than the lightest neutral Higgs boson, while the light h^0 couples to fermions and gauge bosons with a similar magnitude as in the Standard Model. Therefore, in order to verify that the theory is the MSSM, it is necessary to observe the heavier Higgs bosons and measure their couplings.

The dominant mechanisms for producing the heavier Higgs bosons are pair production, $e^+e^- \rightarrow H^0 A^0$ and $e^+e^- \rightarrow H^+ H^-$, and the corresponding mass reach is approximately $\frac{\sqrt{s}}{2}$. The production of a single charged Higgs, $e^+e^- \rightarrow b\bar{t}H^+$, $e^+e^- \rightarrow \tau\bar{\nu}\tau H^+$, and $e^+e^- \rightarrow W^\pm H^\mp$ can

³In non-minimal supersymmetric models, the bound on the lightest neutral Higgs boson mass can be increased to 150 – 200 GeV by assuming that all couplings remain perturbative to the grand unification scale (73).

potentially extend the mass reach, although the rates are rather small (76).

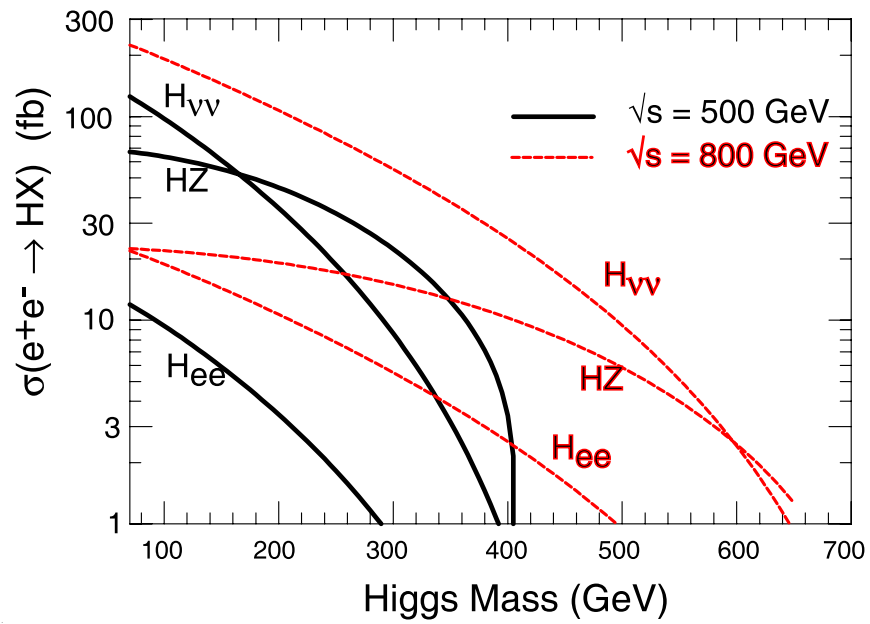


Figure 6: Cross section for the production of a Standard Model Higgs boson through Higgsstrahlung, $e^+e^- \rightarrow Zh$, and in WW and ZZ fusion, $e^+e^- \rightarrow \nu\bar{\nu}h$ and $e^+e^- \rightarrow e^+e^-h$; solid curves: $\sqrt{s} = 500$ GeV, dashed curves: $\sqrt{s} = 800$ GeV. From reference (12).

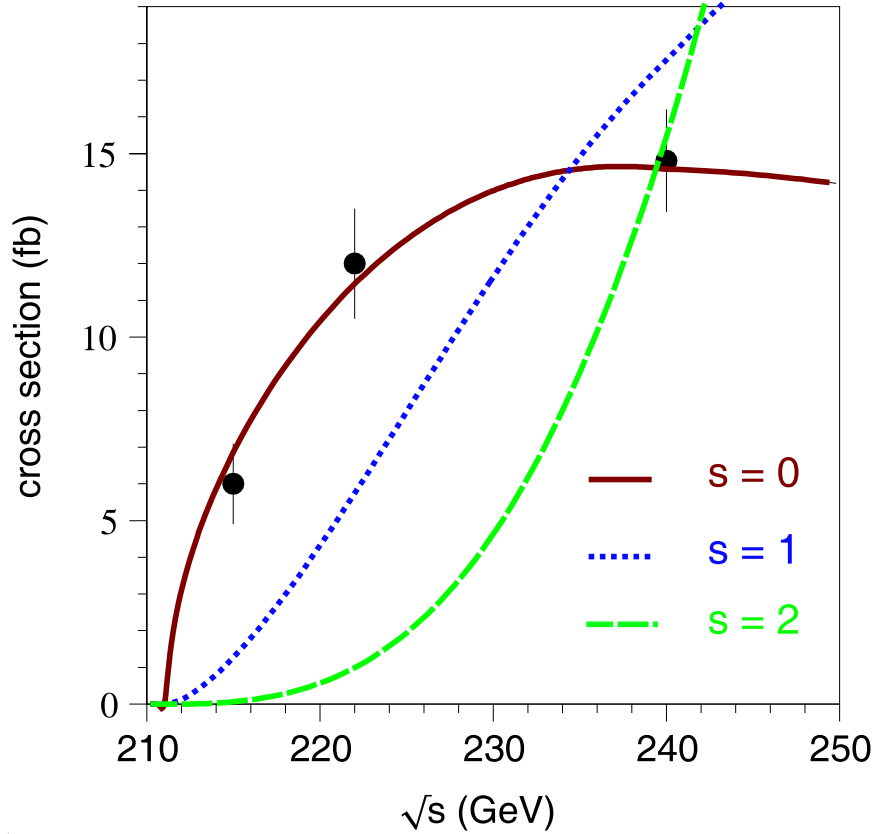


Figure 7: The cross section for $e^+e^- \rightarrow Zh$ as a function of center-of-mass energy for $m_h = 120$ GeV for a spin 0,1, or 2 Higgs boson. An integrated luminosity of $L = 20 \text{ fb}^{-1}$ at each point is assumed. From reference (70).

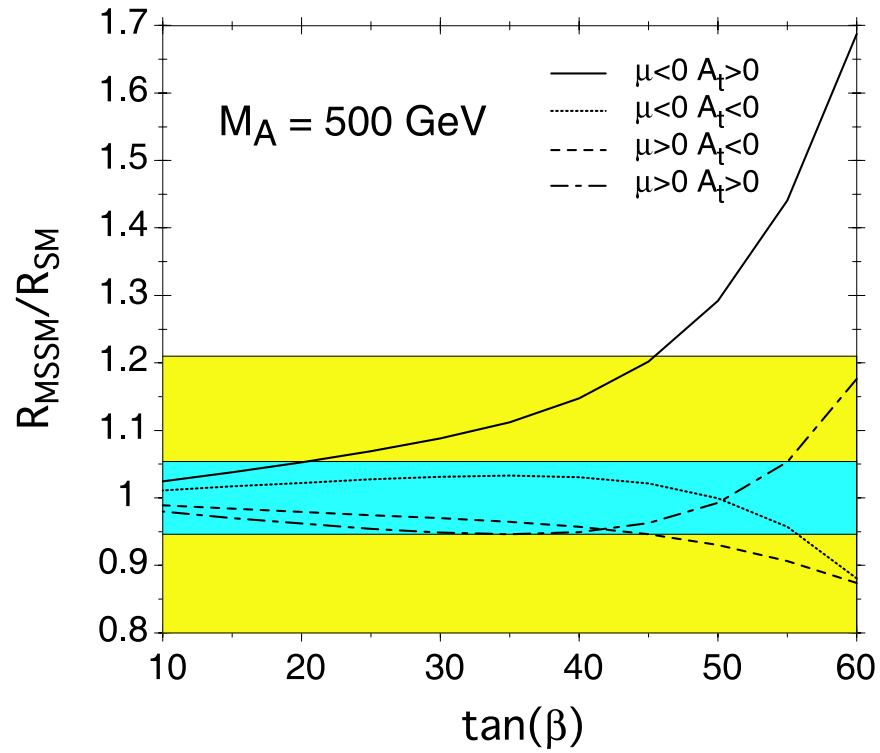


Figure 8: Deviation of the ratio $R \equiv \Gamma(h^0 \rightarrow b\bar{b})/\Gamma(h^0 \rightarrow \tau\bar{\tau})$ from the Standard Model prediction. The expected experimental uncertainty, $\sim 5\%$, is given by the inner bands. From reference (74).

3 Supersymmetry

Supersymmetry is one of the most theoretically motivated extensions of the Standard Model and tremendous attention has been devoted to possible experimental tests (77,78,79). It is a symmetry of space-time relating fermions to bosons and is implemented by associating a new particle differing by one-half unit of spin with every known particle (these particles are collectively dubbed sparticles). Supersymmetric models are very predictive and relate the couplings of the new particles to those of the known particles. This leads to rather generic predictions for the production and decay rates of the sparticles in terms of the unknown sparticle masses.

The Standard Model suffers from a fine tuning problem when quantum corrections to the Higgs boson mass are computed. This problem is cured in a supersymmetric model when the new particles associated with the supersymmetry have masses on the TeV energy scale (80). A linear collider with a center-of-mass energy between $\sqrt{s} = 500 - 1000$ GeV is thus ideally suited to explore the spectrum of a supersymmetric model.

Observing the new particles associated with supersymmetry is a major goal of both the LHC and a linear collider. If supersymmetry is a symmetry at the TeV energy scale, many of the sparticles will be discovered at the LHC (9). At a hadron collider, however, all of the kinematically allowed sparticles will be produced together, and it will be complicated to untangle the pattern of sparticle masses and couplings (81). A lepton collider has the capability to change its center-of-mass energy and so can systematically explore the sparticle spectrum (82). In addition, the scalar sparticles associated with the leptons will be difficult for the LHC to observe and discovery may not occur until the linear collider. The exploration of the spectroscopy of a supersymmetric model will occupy particle physicists at both the LHC and a linear collider for decades, with complementary information gained from the two machines.

A theory with unbroken supersymmetry has particles and sparticles of equal mass. Once the supersymmetry is broken, the sparticles obtain masses which differ from their corresponding particles. Since supersymmetric particles are not observed at the weak scale, supersymmetry must be a broken symmetry. Different mechanisms for breaking the supersymmetry lead to varying patterns of sparticle masses and so understanding the source of the symmetry breaking will be a window to unobserved higher energy scales and to understanding the source of the supersymmetry breaking (77).

Our goals for understanding supersymmetry include (78):

- Find all the predicted sparticles.
- Measure the sparticle couplings and quantum numbers.
- Measure the sparticle masses.
- Understand the supersymmetry breaking scheme.

Supersymmetry associates a new scalar partner with each chiral fermion and so each mas-

sive fermion has two scalar partners: a scalar partner associated with the left-handed fermion and a different scalar partner corresponding to the right-handed fermion. In a model with broken supersymmetry, these scalar partners can have different masses. Each gauge boson has a fermion partner associated with it: the $SU(3) \times SU(2) \times U(1)$ gauge bosons have partners called gauginos with masses M_3, M_2 , and M_1 respectively. The Higgs bosons also have fermion partners (Higgsinos). The charged fermion partners of the W^\pm gauge bosons and the fermion partners of the charged components of the Higgs boson doublets mix to form particles called charginos, $\tilde{\chi}_i^\pm, i = 1, 2$. Similarly, the fermion partners of the neutral Z and γ gauge bosons, and the neutral components of the fermion partners of the Higgs bosons, mix to form mass eigenstates called neutralinos, $\tilde{\chi}_i^0, i = 1, 4$. A general model of supersymmetry breaking allows for arbitrary masses for all of the new superpartners.

The most studied class of supersymmetric models contains a symmetry called R-parity (83). This symmetry requires that supersymmetric particles always be produced in pairs. One consequence of R-parity is that the lightest supersymmetric particle is stable. Since there are stringent experimental limits on stable charged particles, the lightest supersymmetric particle (LSP) is usually assumed to be the lightest neutralino. This particle also provides a viable candidate to explain the dark matter in the universe (24).

Supersymmetric models have been increasingly constrained by measurements of the branching ratio $B \rightarrow s\gamma$, the muon anomalous magnetic moment, $a_\mu = (g - 2)_\mu$, and the measurement of the relic dark matter in the universe (24,25). In some classes of supersymmetric models, these measurements can be interpreted as signals for supersymmetry at the few hundred GeV scale.

The linear collider can pair produce sparticles with masses $M < \sqrt{s}/2$. So the highest possible center-of-mass energy will yield the maximum discovery potential for the new particles predicted by supersymmetric models. The tunable energy of a linear collider allows for a search strategy where the energy thresholds of the sparticles are scanned sequentially. In addition, since the sparticles couple differently to left- and right-handed fermions, polarization of the initial electrons is effective in identifying specific production processes and reducing backgrounds (12,18).

3.1 sleptons

In many models, the scalar partners of the electron (selectrons) and those of the muon (smuons) are the lightest scalar particles. These scalars, collectively termed sleptons, \tilde{l}^\pm , are produced through s -channel γ and Z exchange,

$$e^+e^- \rightarrow \gamma, Z \rightarrow \tilde{l}^+\tilde{l}^-. \quad (6)$$

Selectron pair production receives an additional t -channel contribution from neutralino exchange (84). Sleptons typically decay to either a neutralino, $\tilde{\chi}^0$, or to a chargino, $\tilde{\chi}^\pm$,

$$\tilde{l}^\pm \rightarrow \tilde{\chi}^0 l, \tilde{\chi}^\pm \nu_l. \quad (7)$$

If the slepton decays to the LSP ($\tilde{\chi}_1^0$), the complete decay chain is

$$e^+e^- \rightarrow \tilde{l}^+\tilde{l}^- \rightarrow l^+l^- \tilde{\chi}_1^0\tilde{\chi}_1^0. \quad (8)$$

The momentum of the leptons is precisely measured at a linear collider, while the neutralinos give missing transverse momentum in the detector. In models with R -parity conservation, the lightest neutralino is stable and weakly interacting and is not observed.

The dominant Standard Model background to slepton production and decay to a neutralino is

$$e^+e^- \rightarrow W^+W^- \rightarrow l^+l'^- \nu_l\bar{\nu}_{l'}. \quad (9)$$

The $e^+e^- \rightarrow W^+W^-$ Standard Model background is many times larger than the slepton signal, but since it is strongly peaked in the forward direction, angular cuts are effective in reducing this background. (Because the sleptons are scalar particles, they decay isotropically in their rest frame and so they largely survive the cuts designed to eliminate the W^+W^- background.)

The energy distribution of the outgoing leptons from slepton decay is directly related to the slepton and neutralino masses,

$$\begin{aligned} m_{\tilde{l}}^2 &= \frac{sE_{min}E_{max}}{(E_{min} + E_{max})^2} \\ 1 - \frac{m_{\tilde{\chi}_1^0}^2}{m_{\tilde{l}}^2} &= \frac{2}{\sqrt{s}}(E_{min} + E_{max}), \end{aligned} \quad (10)$$

where E_{max} and E_{min} are the maximum and minimum allowed lepton energies. The endpoints of the lepton energy spectrum can be clearly seen in figure 9, where the distortion in the spectrum is the result of initial state radiation (85). This technique yields measurements of the slepton masses with accuracies in the few hundred MeV range.

Slepton pair production provides an example of the effectiveness of the polarization capabilities of a linear collider for reducing backgrounds. The W bosons couple only to left-handed particles, so scattering right-handed electrons is extremely efficient for reducing the background, as demonstrated in figure 9. One of the definitive predictions of a supersymmetric theory is that of the sparticle couplings. A measurement of the absolute cross section for slepton pair production measures the slepton couplings to 1 – 2% (11).

The slepton masses can also be measured precisely from threshold energy scans. This method is independent of the decay pattern of the sleptons. Since the sleptons are scalars, the threshold energy dependence scales like β^3 , as compared with the β dependence for fermion pair production (where $\beta^2 = 1 - 4M^2/s$ and M is the mass of the produced particle). Measurement of the slepton energy dependence helps to verify that these particles are indeed scalars, as required by supersymmetry.

A linear collider can also run in an e^-e^- mode. This can potentially yield more precise measurements of the slepton masses due to the steeper rise of the $\tilde{e}^-\tilde{e}^-$ cross sections at threshold as compared to e^+e^- collisions (49). Furthermore, the background is expected to be significantly smaller at an e^-e^- collider.

3.2 Charginos and Neutralinos

A linear collider can pair produce both charginos and neutralinos,

$$e^+e^- \rightarrow \tilde{\chi}_i^\pm \tilde{\chi}_i^\mp, \quad i = 1, 2 \quad (11)$$

$$e^+e^- \rightarrow \tilde{\chi}_i^0 \tilde{\chi}_i^0, \quad i = 1, 4. \quad (12)$$

In most models, the lightest neutralino is stable and non-interacting, so direct pair production of the LSP will not be observable. The heavier neutralinos will decay to states including the lightest neutralino. Here we focus on chargino pair production as an example of the capabilities of a linear collider.

Chargino production occurs through s -channel Z exchange and t -channel sneutrino exchange. The charginos decay to final states with multiple jets and missing transverse energy from the unobserved neutralino. The dominant backgrounds are gauge boson pair production, W^+W^- and ZZ , which can be minimized using polarization.

Measurement of the chargino mass probes the entries of the chargino mass matrix: μ , M_2 , $\tan\beta$, and the sneutrino mass which enters into the production cross section. (μ is a Higgs mixing parameter, which is required in order to have electroweak symmetry breaking, M_2 is the mass of the fermionic partner of the W , and $\tan\beta$ is the ratio of the vacuum expectation values of the neutral Higgs bosons.) The chargino mass matrix is

$$m_{\tilde{\chi}^\pm} = \begin{pmatrix} M_2 & \sqrt{2}M_W \sin\beta \\ \sqrt{2}M_W \cos\beta & \mu \end{pmatrix}. \quad (13)$$

The off-diagonal terms are often much smaller than M_2 and $|\mu|$ and in this scenario $m_{\tilde{\chi}^\pm}$ directly measures M_2 or μ .

The chargino mass can be measured through the kinematic endpoints of the decay products and also through a threshold scan. The ability of a linear collider to make an energy scan and to have beam polarization allows a series of measurements,

$$\sigma_L, \sigma_R, A_L^{FB}, A_R^{FB}, m_{\tilde{\chi}^\pm}, \quad (14)$$

where the L, R subscripts denote left- and right- polarized electron beams, and A^{FB} is the forward backward asymmetry. σ_R contains only the contributions from γ and Z bosons, while σ_L is sensitive to t -channel sneutrino exchange. The combination of these measurements allows for a complete exploration of the parameter space in the chargino sector.

3.3 *mSUGRA*

One of the most widely studied supersymmetric models is the mSUGRA, or minimal supergravity, model (86). This model has the practical advantage that it is extremely restrictive, with all masses and mixing parameters being predicted in terms of four input parameters and a sign. The model assumes that the mass of all of the new scalar sparticles are given by a single parameter, m_0 , at the grand unification scale, $M_{GUT} \sim 2 \times 10^{16} \text{ GeV}$ (M_{GUT} is defined to be the energy scale where the 3 gauge coupling constants meet). The gauginos are likewise assumed to have a common mass, $M_{1/2}$, at the GUT scale. At the scale M_{GUT} , the theory is completely specified by,

$$m_0, M_{1/2}, A_0, \tan \beta, \text{sign}(\mu). \quad (15)$$

All of the sparticle masses and mixings can be expressed in terms of these variables.

Renormalization group equations are used to evolve all parameters to the weak scale. At this scale, the gaugino masses are predicted to be in the ratio,

$$M_1 : M_2 : M_3 = 1 : 2 : 7 \quad . \quad (16)$$

Measurement of gaugino parameters in these ratios would be a strong indicator for the mSUGRA type models. Typically in mSUGRA models, the lightest scalars are the sleptons and over much of the parameter space, the lightest supersymmetric particle is the neutralino.

The discovery reach of a collider in the mSUGRA model can be conveniently expressed in terms of its reach in the $m_0 - M_{1/2}$ plane for fixed values of A_0 , $\tan \beta$, and $\text{sign}(\mu)$ (87). An example of such a reach plot is shown in figure 10. It is interesting to note that there is a region of parameter space (large m_0 and moderate $M_{1/2}$) which is inaccessible to the LHC, but which a 1 TeV linear collider can explore (88). This region is particularly interesting because the parameters allow the neutralino to be a dark matter candidate consistent with astrophysics experiments (24).

3.4 *Gauge Mediated Supersymmetry Breaking*

In this class of supersymmetric models, the supersymmetry breaking is communicated from a hidden sector by the gauge interactions of a new type of particle called a messenger field. Gauge mediated models (89) have a distinctive pattern of masses: gaugino masses arise at one loop and are proportional to the gauge coupling constants,

$$M_i \sim \frac{\alpha_i F}{4\pi M} \quad (17)$$

and scalar masses arise at two-loops

$$M_{scalar}^2 \sim \sum_i C_i \left(\frac{\alpha_i}{4\pi} \right)^2 \left(\frac{F}{M} \right)^2 \quad (18)$$

where \sqrt{F} is the scale of supersymmetry breaking, M is the messenger mass, and c_i depends only on the gauge quantum numbers of the scalar. This type of model yields a hierarchy between the strongly interacting squarks and gluinos and the weakly interaction sparticles. Confirmation of this pattern of masses at a linear collider would be a signal for gauge mediated supersymmetry breaking.

3.5 *Extracting the Underlying SUSY Parameters*

If evidence for supersymmetry is discovered at either the LHC or at a linear collider, the next goal will be to understand the source of supersymmetry breaking. This symmetry breaking presumably occurs at a high energy scale. As we have seen, the pattern of sparticle masses can be quite different depending on the source of the supersymmetry breaking. Precise measurements of SUSY masses and couplings can be used to extrapolate from the weak scale to high energy using renormalization group techniques. Because the evolution of the masses and couplings with energy is sensitive to the underlying model, such an exercise offers a window to the Planck mass scale.

The evolution of the gaugino masses is particularly interesting, since in many models the ratio of gaugino masses is predicted to be that of Eq. 16. Figure 11 (from (90)) shows the evolution of gaugino masses in an mSUGRA model, assuming the precision which can be obtained in a linear collider for the measurements of M_1 and M_2 . Note that M_3 , the mass of the gluino, cannot be measured at a linear collider, but must be determined at the LHC. Similar plots can be made for the evolution of the scalar masses. The combination of a linear collider with the LHC will truly probe the high energy/GUT scale (27).

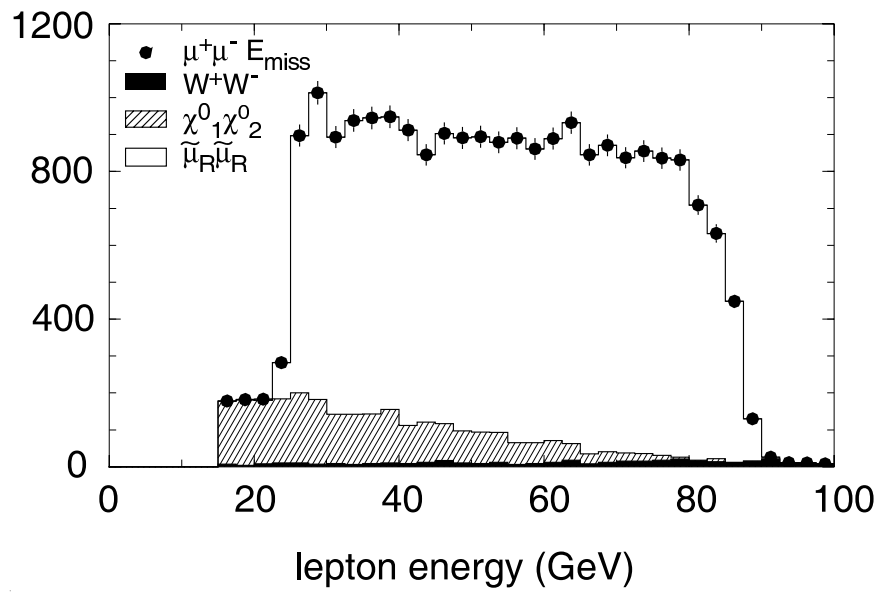


Figure 9: Signal from $e^+e^- \rightarrow \tilde{\mu}_R^+ \tilde{\mu}_R^- \rightarrow \mu^+ \mu^- \tilde{\chi}_1^0 \tilde{\chi}_1^0$ and the dominant backgrounds for $m_{\tilde{\mu}_R} = 132$ GeV and $m_{\tilde{\chi}_1^0} = 71.9$ GeV, $\sqrt{s} = 320$ GeV, and an integrated luminosity of $L = 160$ fb $^{-1}$. From reference (85).

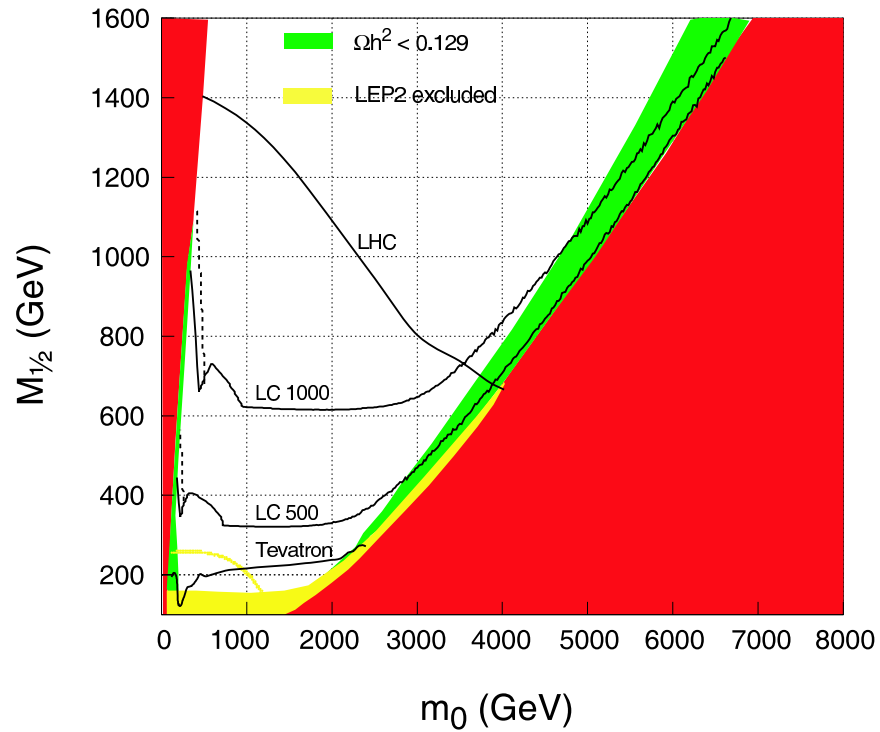


Figure 10: *Discovery reach of a $\sqrt{s} = 500$ GeV and 1 TeV linear collider for the mSUGRA model with $\tan \beta = 30$, $A_0 = 0$, and $\text{sign}(\mu) = +$. The discovery reach of the Fermilab Tevatron with an integrated luminosity of 10 fb^{-1} , and the LHC with 100 fb^{-1} are also shown. The green shaded region is that preferred by dark matter experiments, while the brown region is theoretically inconsistent. From reference (88).*

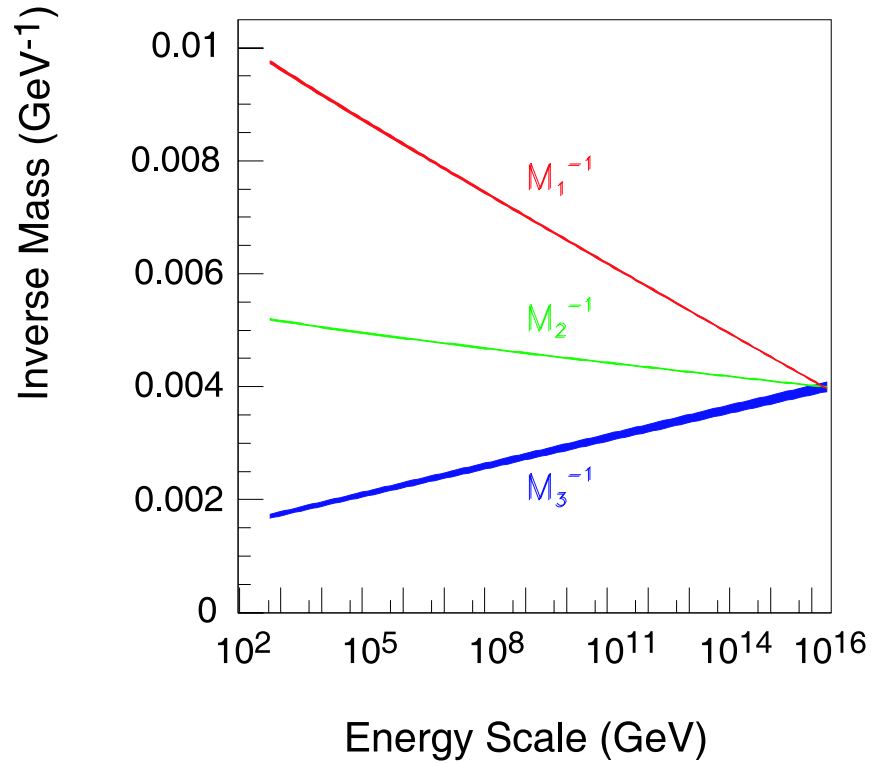


Figure 11: Evolution of the gaugino masses in an $mSUGRA$ model. The width of the band is the 1σ confidence level assuming the experimental accuracies expected at the LHC for M_3 and a linear collider for M_1 and M_2 . The $mSUGRA$ point is $m_0 = 200$ GeV, $m_{1/2} = 250$ GeV, $A_0 = -100$ GeV, $\tan \beta = 10$, and $\text{sign}(\mu) = +$. From reference (90).

4 Other Extensions to the Standard Model

4.1 Strongly Interacting Electroweak Symmetry Breaking

Although the precision measurements shown in figure 1 strongly indicate the presence of a light Higgs boson, or something like it, it is possible that the electroweak symmetry breaking results from a new strong interaction, such as technicolor (20), a composite Higgs theory, or even something completely different than the Standard Model. Theories with a heavy Higgs boson, or with no Higgs boson, can be parameterized in terms of effective Lagrangians, where the operators \mathcal{O}_i are constructed from the Standard Model fields and required to be invariant under the $SU(3) \times SU(2) \times U(1)$ gauge groups. The effective Lagrangian describes physics at the weak scale and the new physics which replaces the light Higgs boson of the Standard Model is contained in higher dimension operators which then depend on the scale at which the new physics is introduced, Λ ,

$$\mathcal{L} \sim \mathcal{L}_{SM} + \sum_i \frac{f_i}{\Lambda^2} \mathcal{O}_i + \dots \quad (19)$$

Fits to precision electroweak measurements allow a heavy Higgs boson with a mass $M_h \sim 400$ - 500 GeV, with new physics at the scale $\Lambda \sim \mathcal{O}(1 - 3)$ TeV (91). Similarly, the Higgs boson can be removed completely from the theory with new physics occurring through the operators of Eq. 19 at the TeV scale (91). In both the case with a heavy Higgs boson and where there is no Higgs boson, the three- and four-gauge boson interactions will differ from those of the Standard Model by terms which scale as powers of $1/\Lambda$.

If the Higgs boson is heavy, $M_h \sim 400$ GeV or larger, there is no distinct Higgs resonance, since the Higgs boson width grows with the Higgs mass. A heavy Higgs boson implies that the self-interactions of the W and Z gauge bosons are becoming strong (7). The measurement of the branching ratios, $h \rightarrow W^+W^-$ and $h \rightarrow ZZ$, would be sensitive to this physics and could help to untangle the underlying mechanism of symmetry breaking (92). If the Higgs boson is removed completely from the theory, or is very heavy, then the effects will be seen in non-Standard Model self-interactions of the W and Z gauge bosons. Changes to the 4-gauge boson vertices can be probed by measuring gauge boson scattering through the processes, $e^+e^- \rightarrow \nu\bar{\nu}W^+W^-$ and $e^+e^- \rightarrow e^+e^-ZZ$. These effects are suppressed by powers of the scale Λ and are expected to be small (12). Probing the 4-gauge boson vertices requires that the linear collider run at the highest possible energy and with the highest possible luminosity.

Strong interactions in the electroweak sector can also manifest themselves through alterations of the 3-gauge boson vertices. The process $e^+e^- \rightarrow W^+W^-$ is sensitive to alterations in the γW^+W^- and ZW^+W^- vertices. Since W^+W^- pair production pairs is the largest single contribution to the total e^+e^- cross section, this process is quite sensitive to small changes in the 3-gauge boson vertices (12,11). In addition, in many models with strong electroweak symmetry breaking, there is a ρ -like resonance with a mass below a few TeV whose properties can be modeled by anal-

ogy with QCD. A linear collider running at $\sqrt{s} = 800$ GeV and with an integrated luminosity of $L = 500 \text{ fb}^{-1}$ can see the effects of a 1-2 TeV resonance through the process $e^+e^- \rightarrow W^+W^-$ (16) as is shown in figure 12.⁴ A linear collider can even probe the scenario where the Higgs boson is removed from the theory by becoming infinitely massive (the point labelled LET in figure 12).

In order to go beyond the effective Lagrangian approach, it is necessary to construct explicit models which allow for a heavy Higgs boson, or no Higgs boson, and are consistent with the precision electroweak measurements. These models tend to have new light vector bosons or fermions whose effects could be observed at a linear collider (93).

4.2 Top Mass measurements

A linear collider, operating near the $t\bar{t}$ production threshold energy, will have broad capabilities for precision top quark measurements. Measurements include the top quark mass, m_t , and width, Γ_t , along with the top quark- Higgs boson Yukawa coupling, g_{tth} (94,95). The large top quark mass gives the top quark a special role in many models with physics beyond the Standard Model and so precise measurements of its parameters will provide important new insights into the source of mass (19). The top quark mass is also an important component of the electroweak precision measurement program, as seen in figure 1, and so it is important to measure it as accurately as possible.

Because of its large width, $\Gamma_t \sim 1.5$ GeV, the top quark will decay before it hadronizes and so non-perturbative effects are expected to be highly suppressed. The dependence of the cross section for $e^+e^- \rightarrow t\bar{t}$ on the energy can be computed reliably and the rate increases by a factor of ten as the center- of- mass energy is varied by 5 GeV around the threshold energy. The location of the rise of the cross section can be used to extract the top quark mass, while the shape and normalization yield information about Γ_t , g_{tth} , and α_s . The threshold cross section has been calculated including some of the next-to-next-to-leading logarithms, as shown in figure 13 (96,97). The complete set of next-to-next-to-leading logarithmic contributions is not yet complete, but the large size of the corrections relative to the next-to-leading logarithmic terms (98) suggests that the uncertainty on the cross section measurement will be slightly larger than previously estimated, $\delta\sigma_{t\bar{t}}/\sigma_{t\bar{t}} \sim \pm 6\%$. This implies that a linear collider operating at the $t\bar{t}$ threshold will be able to measure the top quark mass with an accuracy of $\delta m_t \sim 100$ MeV (95). This should be compared with an expected accuracy at the LHC of $\delta m_t \sim 1\text{-}2$ GeV (9).

4.3 Extra Dimensions

An alternative solution to the hierarchy problem was discovered in 1998 (99) through the realization that an effective Planck scale with electroweak energy can exist as a fraction of the true Planck

⁴When the W^+W^- interactions become strong, the amplitude for $e^+e^- \rightarrow W^+W^-$ develops a complex form factor, F_T . Figure 12 shows the predictions for this form factor in a model with a heavy vectorlike ρ meson.

energy if there are extra spatial dimensions. There are now three classes of these extra-dimension models, differing from each other in the geometry of the various fields. They also have different experimental signatures (100). Common features of the models are closely-spaced excitations extending into the TeV mass range and particles with spin-2, both well suited for study in e^+e^- collisions at the highest possible energies. Furthermore, the e^-e^- , $e^-\gamma$, and $\gamma\gamma$ options of a linear collider (101), as well as the possibility of transverse polarization (102), are uniquely suited to differentiating the extra-dimension models.

The original extra dimensions model was described by Arkani-Hamed, Dimopoulos, and Dvali (ADD) (99); it confines the Standard Model fields to a 1+3 dimensional brane, while gravity propagates in the “bulk” of the other dimensions. In this way, gravity might be strong in the bulk, but only a fraction is felt on the brane. It can be arranged so that d of the dimensions forming the bulk share a relatively large length scale R , with the result:

$$M_{planck}^2 \sim M_{brane}^{d+2} R^d, \quad (20)$$

where M_{brane} is the effective Planck mass scale on the 3-brane where the Standard Model lives. Thus, the effective Planck mass can be tuned TeV scale; for $d=2$, R is on the order of a millimeter. Unfortunately, ADD introduces a new hierarchy problem insofar as the TeV string scale is so different from the compactification scale. A consequence of the graviton propagating in the bulk is a tower of excited Kaluza-Klein (KK) graviton states which couple weakly to Standard Model particles. In e^+e^- collisions the experimental signature is either missing energy in Standard Model processes by radiation of a KK graviton from SM particles (103), or altered pair production by virtue of a graviton propagator (104, 105, 106, 107, 108) (the pair rate and angular distribution would be affected). A striking signature would be radiation of a graviton from a virtual photon, creating a visible photon and missing energy (109, 110). Figure 14 shows a calculation (111) for the radiated graviton in Bhabha scattering. Clean measurement of the angular distribution of final states consisting of a single photon and missing energy should be able to distinguish the ADD model from a scenario where the missing energy is from extra neutrinos or superpartners.

A different model due to Randall and Sundrum (RS) (112) allows for a brane having a TeV scale without requiring the compactification radius of the extra dimensions to be large and cures the ADD heirarchy problem. In the RS schemes there is one extra dimension and there are two branes, one with an effective Planck mass (\bar{M}_{planck}) which can be the TeV scale, and the other at the Planck scale; a scalar field in the bulk is needed to keep the branes the proper distance apart. This results in a factor $e^{-\pi\kappa R}$ which warps the spacetime metric and creates the scale difference between the two branes; κ is the curvature of the fifth dimension and R is the compatication scale. Since the metric is a function of the 5th coordinate, the theory is nonfactorizable. A TeV scale can be achieved on the low energy brane if $\kappa R \sim 12$. The original models had the Standard Model particles located on the TeV brane, but current models let all particles apart from the Higgs boson reside in the bulk. As in the ADD case, the extra dimension gives rise to KK excitations of the Standad Model particles. Unlike ADD, the graviton masses are of the electroweak scale,

and there will be a series of KK gravitons. The masses of the KK excitations of the gravitons are $M_n = \zeta_n m_0$, where $m_0 = \kappa e^{-\pi\kappa R}$ and ζ_n are zeroes of the Bessel function (113); other schemes lead to different mass spacings. It is perhaps more useful to consider the free model parameters as m_0 and $c = \kappa/\bar{M}_{plank}$ which is an effective coupling (114). The gravitons have weak strength and decay into pairs of Standard Model particles with a width dependent on c_0 . Figure 15 shows a spectrum of such KK excitations, clearly well suited to the excellent mass resolution of a linear collider. These KK resonances resemble excited Z bosons. The key RS experimental signature is the spin-2 nature of the RS gravitons, which is reflected in the angular distributions and often with an enhancement of particles transverse to the beams. Figure 16 summarizes the difference between ADD and RS production of single photons versus dimuons. At the very high energy scale of $\sqrt{s}=2$ TeV shown in this figure, it is possible for a linear collider to distinguish between these two extra dimension scenarios.

The RS bulk scalar field gives rise to a projection on the TeV brane; the resulting particle is dubbed the “radion” (115). The radion manifestation of the scalar field should also have clear experimental consequences due to its Higgs-like nature. The radion field therefore mixes with the Higgs boson and can significantly change the Standard Model Higgs boson branching ratios.

There is also the possibility that all of the Standard Model fields live in the extra-dimensional bulk, in which case all Standard Model particles will have KK excitations; such models are called Universal Extra Dimensions (UED) (116). In UED models, because all the fields are allowed in the bulk, conservation laws apply with the consequence that there is KK number conservation. At lowest order, excited particles are produced in pairs, and the lightest KK particle is the photon with $n=0$. With excitations possible for all particles, the phenomenological space is large and more study is encouraged. This model is actually very similar to SUSY insofar as every SM particle has a tower of KK-partners; in contrast to SUSY, the partners have the same spin. Determining whether one is seeing UED or SUSY will require excellent determination of angular distributions. In the UED models there can be excited quark bound states resulting in a complex spectrum (117).

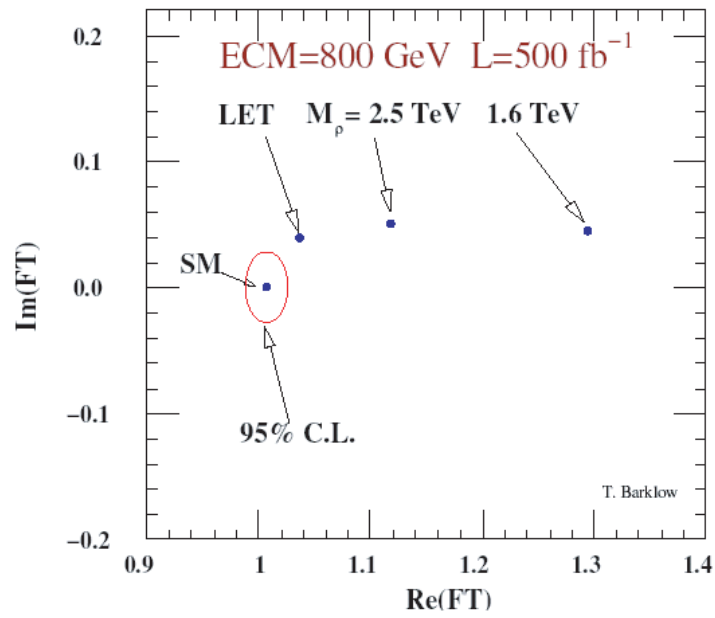


Figure 12: Sensitivity of the longitudinal W form factor at a linear collider with $\sqrt{s} = 800$ GeV and an integrated luminosity of $L = 500$ fb⁻¹ to a “ ρ ”-like resonance of mass 1.6 and 2.5 TeV. Also shown is the Standard Model result and the result in a theory where the Higgs mass is taken to be infinitely massive (labelled *LET*). From reference (12).

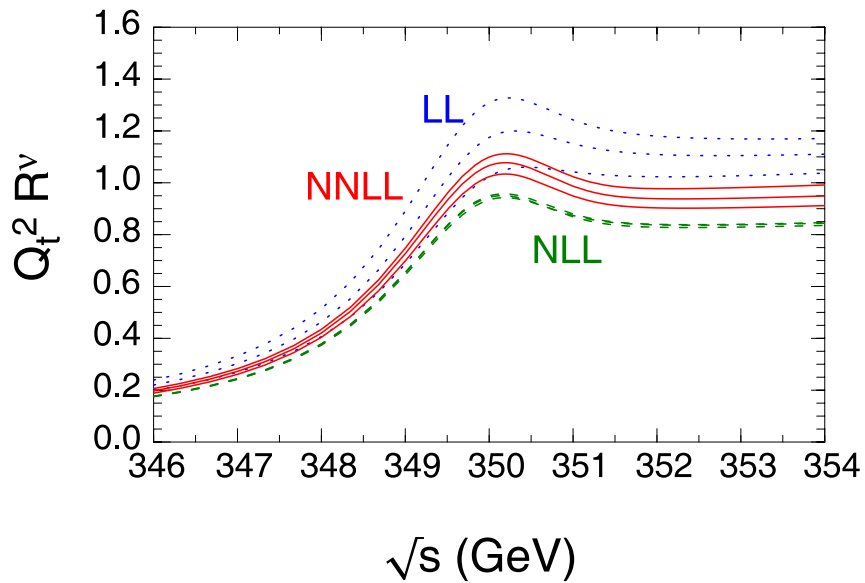


Figure 13: Dependence of the $e^+e^- \rightarrow t\bar{t}$ cross section on the center-of-mass energy, \sqrt{s} . The curves labelled LL (dotted), NLL (dashed), and NNLL (solid) include leading logarithmic, next-to-leading logarithmic, and next-to-next-to-leading logarithmic contributions, respectively. The three curves for each set of corrections represent the variation of the rate with changes of the renormalization scale. This figure uses a threshold mass definition for the top quark mass (97). From reference (96).

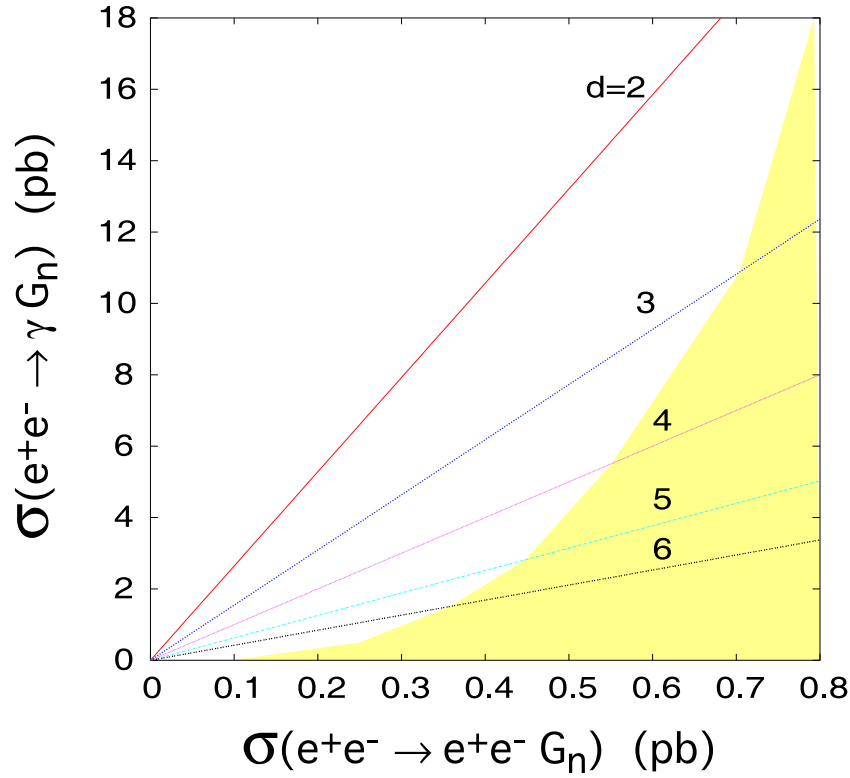


Figure 14: Cross section for $e^+e^- \rightarrow \gamma G_n$ versus $e^+e^- \rightarrow e^+e^- G_n$ for polarized electrons at $\sqrt{s} = 500$ GeV; G_n are the KK excitations of the gravitons. The number of extra dimensions is indicated by the number on each curve. The shading represents the region of low reliability for the theoretical calculation. From reference (111).

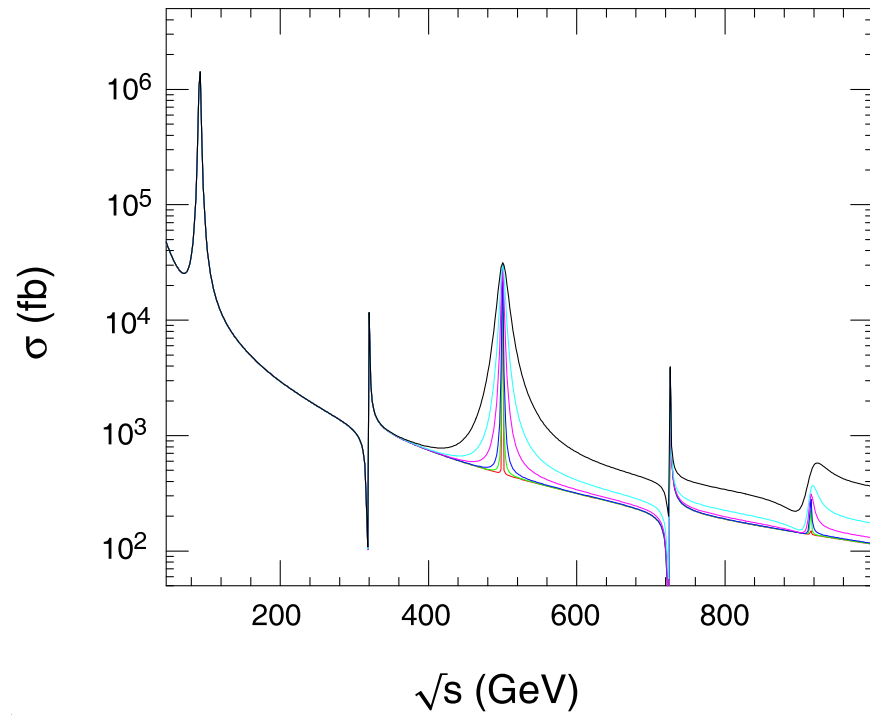


Figure 15: e^+e^- production of graviton and neutral gauge KK excitations for a model having the first KK excitation at 500 GeV. The series of curves represents various values of κ/\bar{M}_{planck} . From reference (113).

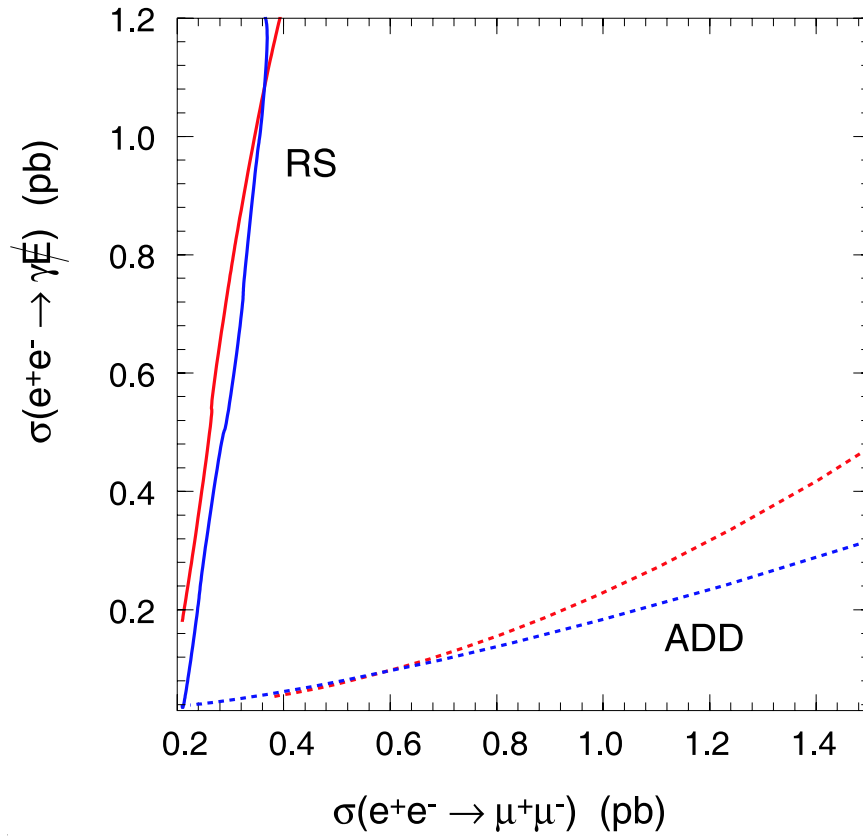


Figure 16: Cross section for single photon production compared to the dimuon production for some ADD and RS models in e^+e^- production at $\sqrt{s} = 2$ TeV. The two ADD lines are for extra dimensions of 3 and 6. The RS curves are for $m_0 = 200$ and 400 GeV. From reference (114).

5 The Linear Collider and Cosmology

5.1 *The Linear Collider and Astrophysics*

Two startling discoveries in astrophysics have presented High Energy Physics with new challenges. Astrophysical measurements indicate that 95% of the gravitating energy in the universe is of an unknown form (23). Even more embarrassing is the indication that $\sim 70\%$ of the closure density of the universe is a dark energy heretofore unpredicted in any physical theory (except for Einstein's cosmological constant) (118). These conclusions result from a number of remarkably consistent astrophysical measurements. Measurement of the Cosmic Microwave Background (CMB) (119) gives the photon density of the universe. Together with a value for the Hubble expansion parameter, measurement of the CMB temperature anisotropy directly measures the total matter+energy density Ω_{tot} (scaled by the critical density) as well as the density for baryonic matter Ω_B . The baryonic matter is that from all strongly interacting particles; their density (relative to the photons) is also inferred from measured isotopic abundances interpreted via big-bang nucleosynthesis. The total matter density can be inferred from the speed distribution of luminous matter within galactic clusters, gravitational lensing, and features in the CMB anisotropy. The dark energy is indicated by nonlinearity in the luminosity-distance curve measured for Type Ia supernovae (120). Combining the experimental data yields the values 0.044 ± 0.004 for the baryonic matter density, 0.22 ± 0.02 for the dark matter density, and 0.73 ± 0.04 for the dark energy component (121, 122, 25, 123). The remaining 0.006 constitutes neutrinos and photons. One particular example of the parameter space is illustrated in figure 17 (from reference (124)).

The connections to particle physics are obvious. Candidates for the dark matter exist in a number of the extensions to the Standard Model. The dark energy issue is tougher to understand, but it could possibly be explained by evolution of the vacuum. The connection between High Energy Physics and cosmology is not limited to dark matter and dark energy. The Standard Model in its minimal form fails to explain the lack of observed antimatter in the universe. It is possible that this asymmetry is created at the weak scale and so linear collider physics could shed light on the problem. The spectrum of cosmic rays at ultra-high energy (10^{19} eV and higher) is not fundamentally understood and could have its roots in electroweak physics. In the following sections, we discuss the implications for LC physics of the astrophysics connections.

5.2 *Dark Matter*

Candidates for dark matter (125, 78) abound in the new theoretical extensions to the Standard Model, and the role of the LC would be to identify the creation of such particles and show that the annihilation cross sections, σ_A , are consistent with the astrophysical measurements. The only thing we know about the dark matter is that it must be neutral and its abundance, which can be related to its production cross section. Within the context of cosmological evolution (the big bang

coupled with an electroweak phase transition leading to inflation), particles are in equilibrium as long as their interaction rate with the cosmic plasma is larger than the Hubble expansion. When the interaction rate falls below the expansion rate of the universe, these particles are said to “freeze out”, implying that their comoving number density becomes reasonably constant. For relativistic particles of mass m , the number density after freeze-out will be similar to that for the photons, with $\Omega h^2 \sim m/(100 \text{ eV})$, where h is the Hubble constant in units of 100 km/s/Mpc. This cannot account for the measured dark matter abundance, so we must consider nonrelativistic particle freeze-out. For particles which are nonrelativistic at the time of decoupling, iterative solution of the Boltzmann equation yields $\Omega \sim 400 \text{ fb}/\sigma_A$ (126,23). Equating this to the measured 0.22 indicates that the dark matter is nonrelativistic, or cold (CDM), and has an annihilation cross section in the weak interaction range.

There is a growing list of candidates to account for the CDM: weakly interacting massive particles (WIMPs), the gravitino, axions, super-weakly interacting particles, other non-WIMP matter, and excitations arising in extra-dimension models. The axion is a long-lived pseudo-Nambu-Goldstone boson invented as a possible solution of the strong CP problem (127). Axions have very small couplings to matter and therefore cannot be effectively probed at particle colliders. The lightest particles in Universal Extra Dimension theories (Kaluza-Klein towers or brane excitations) are newer candidates for the CDM (128,129,130). If these candidates have masses in the electroweak mass range, the superior mass resolution of a linear collider would identify the series of narrow states associated with these dimensional excitations. WIMPs are the dark matter candidates for which the LC role has been most studied so far. WIMP CDM candidates include supersymmetric particles (131), with the best candidate for CDM being the lightest supersymmetric particle (LSP), which is stable owing to R-parity conservation. If SUSY breaking is gauge-mediated, the LSP is the gravitino, which would interact at gravitational strength. This scenario would be born out experimentally by identifying the other superparticle masses and couplings.

To demonstrate that an LSP constitutes the CDM, the correct freeze-out density must be achieved through the possible annihilation and production scattering processes. Neutralino annihilation occurs both through self-annihilation and by scattering with other superpartners (coannihilation) such as staus. The supersymmetric particle spectra can complicate the freeze-out scenario significantly, therefore associating the LSP with the CDM will require detailed knowledge of the supersymmetric particle masses and couplings. For instance, if the LSP has a slightly heavier partner with the same quantum numbers and a larger annihilation cross section, the effective LSP annihilation rate is significantly altered. Simply knowing the LSP mass and self annihilation cross section is not good enough to identify this as the CDM, and this stresses the need for precision measurements in this physics. The neutralinos are ideal objects to study at the linear collider. The masses will be measured to high precision via the kinematics, and measurement of the production rates from polarized beams will absolutely establish their gaugino properties. High precision measurements afforded by a linear collider can determine the effective Ω_{DM} to an accuracy nearly equalling that for the astrophysical measurements (132).

As an example of how the supersymmetric parameter space can be studied in the context of CDM, we focus on the supergravity models (see section 3.3). In minimal supergravity (mSUGRA) one assumes a single common gaugino mass $M_{\frac{1}{2}}$ and a universal trilinear term A_0 . The only remaining parameters of this model are the soft scalar mass m_0 , the ratio of Higgs field vacuum expectation values $\tan\beta$, and the sign of the Higgs mixing mass μ . For assumed values of $\tan\beta$, A_0 , and $\text{sign}(\mu)$, the LSP production can be calculated in the m_0 - $M_{\frac{1}{2}}$ space to derive values of $\Omega_{DM}h^2$; this is shown in figure 18 for $A_0=0$ and $\mu > 0$.

To explore the mSUGRA possibilities, it is useful to describe regions of distinct LSP production and annihilation which can support the observed CDM equilibrium density. Figure 19 (adapted from (133, 88, 13)), shows the allowed m_0 - $M_{\frac{1}{2}}$ space after applying restrictions for the feasibility of electroweak spontaneous symmetry breaking and CDM constraints. There are four distinct LSP production regions. In the low mass bulk area the parameters of the supersymmetric model are moderate and in a range where the symmetry breaking does not result from fine-tuned cancellations between very large sparticle masses. In this region the LSP is the fermion partner of the U(1) gauge boson (the Bino), and the model has light sleptons which allow t-channel annihilation to keep Ω_{DM} in the allowed range. The “co-annihilation” region is where the LSP is near-degenerate with other sparticles, enhancing the annihilation reaction. The “focus point” region at $m_0 \gg M_{\frac{1}{2}}$ has the fermion partner of the neutral Higgs boson (Higgsino) as the LSP; here annihilation is enhanced by Z exchange. The “Higgs annihilation” region is where s-channel annihilation becomes enhanced for $M_h \sim 2M_{LSP}$. These regions are indicated in the figure, along with letters indicating suggested benchmark points for studying the possible scenarios (13).

5.3 Baryogenesis

Standard Model physics cannot explain the observed matter/antimatter asymmetry of the universe. The theoretical recipe for generating a baryon asymmetry was pointed out by Sakharov (134) as requiring violation of baryon number, violation of the C and CP symmetries, and a departure from thermal equilibrium. These conditions are possible in GUT-scale processes (135), but physics at this scale is not testable in particle accelerators. However, since there is already speculation that supersymmetry is broken at the electroweak scale, electroweak physics does provide several possibilities for baryogenesis which a linear collider could probe.

In electroweak theory baryon number can be violated by nonperturbative processes arising from the nontrivial structure of the electroweak vacuum (136). A phase transition in the Higgs field could give rise to baryogenesis at TeV temperatures. The order of the transition is determined by the modulus of the Higgs field and the critical temperature is that where the nonzero minimum of the Higgs field becomes the favored vacuum state. Thermal equilibrium is disrupted by quantum-tunnelling nucleation of bubbles of the new vacuum state, and these bubbles eventually expand and carry the phase transition to all space. CP is violated during the periods of phase change

as the Higgs field is changing. Within the minimal Standard Model it is not possible to achieve the fundamental criterion $\frac{v}{T_c} > 1$. The MSSM can satisfy the condition, though there are tight theoretical constraints: $M_h < 120$ GeV and $m_{stop} < m_{top}$ for $\tan\beta > 5$ (137), however others are less optimistic (138). The precision measurements from a linear collider of the stop mass and mixing parameters are essential for probing electroweak baryogenesis. The CP constraints would be obtained from precision measurement of chargino and neutralino masses and mixings.

There are other mechanisms for baryogenesis worth mentioning. In leptogenesis (139) a lepton asymmetry creates a baryon asymmetry via EW processes. The Sakharov criteria are satisfied by the decay of a heavy lepton which has frozen out of thermal equilibrium. Such heavy leptons could be, e.g., a right-handed Majorana neutrino which violates the B-minus-L conservation. The SM can be extended to accommodate such particle by embedding in the GUT group SO(10), which is already an attractive way to describe the smallness of neutrino masses. The linear collider could shed light on this scenario by accessing GUT-scale physics via precision electroweak measurements or by direct observation of lepton flavor violation. Affleck and Dine (140) have suggested a scheme for baryogenesis from the decay of scalar cosmological fields carrying nonzero baryon number. The MSSM facilitates the mechanism nicely, providing yet another theoretical scenario requiring precision measurements in the electroweak sector.

5.4 Dark Energy

The fact that most of the energy density in the universe is neither in the form of matter or radiation is undeniable from the case made with data from the Type Ia supernova survey, fits to the CMB anisotropy, and the clustering properties of radio galaxies. The source of this dark energy remains a mystery. Some possible explanations are exotic supersymmetry breaking, extra-dimensions, scalar fields with both kinetic and potential terms in the Lagrangian, and modifications to gravity. Of these, the first three might be resolved with linear collider data.

If supersymmetry broken at the electroweak scale were the correct theory, the dark energy should be at the supersymmetry breaking energy scale of 1 TeV. The vacuum energy density is $\rho_{vac} = E_{vac}^4 = (10^{-3} \text{ eV})^4$, so the theory differs with observation by 15 orders of magnitude (23). But perhaps supersymmetry is broken differently. Discovering supersymmetry and performing precision measurements leading to a understanding of the breaking might lead to understanding of the dark energy.

In some models with extra dimensions, the spatial geometry contributes to the apparent 3D vacuum energy significantly. For instance, in brane models with two extra dimensions, the brane tension affects the observed cosmological constant. If the extra dimensions are sufficiently large, a linear collider could shed light on the dark energy problem by mapping out the spectrum of Kaluza-Klein excitations.

The dynamical scalar field in models like quintessence (136) interacts with matter. The dark energy can therefore interact with the dark matter, and if the dark matter is in the form of,

e.g., neutralinos, measurements of the supersymmetric particle masses might again shed light on the dark energy.

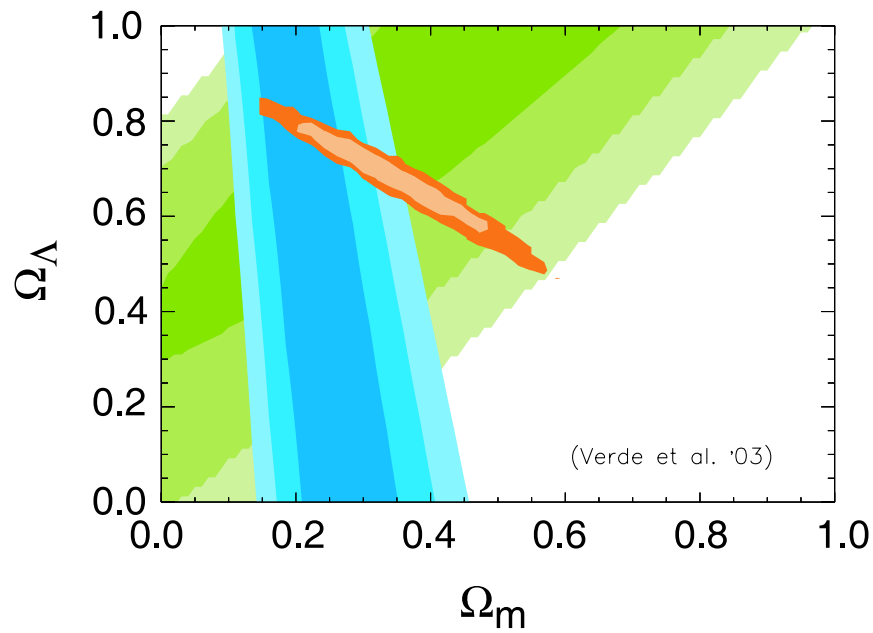


Figure 17: *The one and two standard deviation contours of experimental data in $\Omega_\Lambda - \Omega_m$ space. The broad band with positive slope represents supernova data. The narrow band with negative slope comes from CMB anisotropy measurements. The vertical band is from the 2° field galaxy survey. From reference (124).*

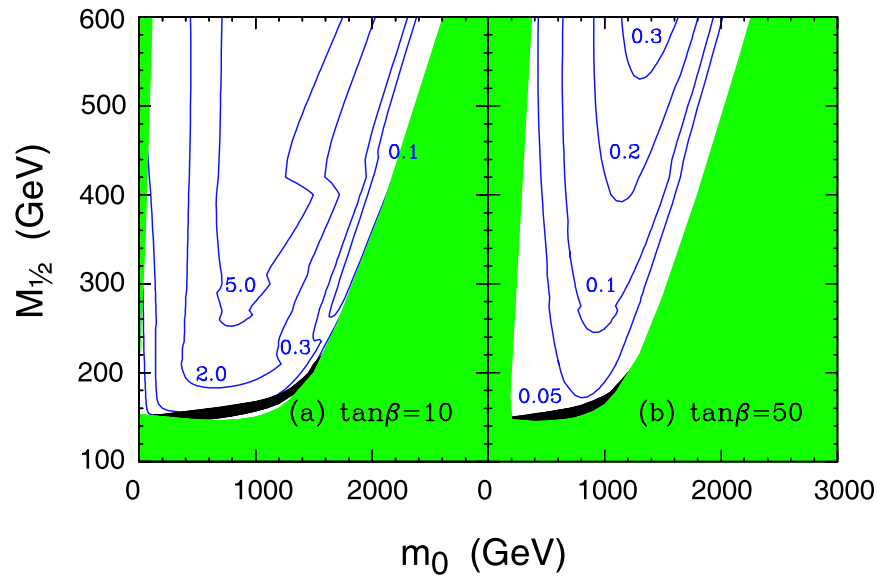


Figure 18: *Contours of Ωh^2 in the $mSUGRA$ model. Here $A_0 = 0$ and $\mu > 0$; representative values of $\tan\beta$ are as indicated. The shaded regions are excluded by the requirements of a neutral LSP (left) and the 103 GeV chargino mass bound from direct searches at the Tevatron (right and bottom). In the black region, neutralinos annihilate through the light Higgs pole. (Heavy Higgs poles also play a role in limited regions with $\tan\beta = 50$ and $m_0 < 1$ TeV.) Effects of co-annihilation, important along the boundaries of the excluded regions, have not been included. From reference (126).*

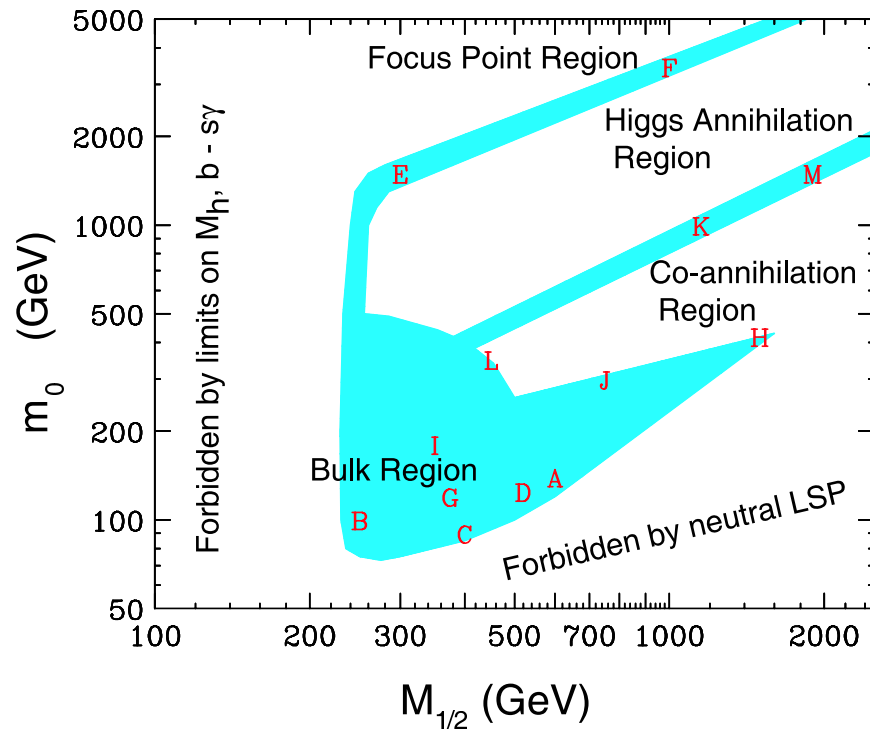


Figure 19: Allowed regions for m_0 versus $M_{1/2}$ in $mSUGRA$ models. The various labelled regions are described in the text. Also shown are benchmark points for studying various types of supersymmetric model. Adapted from references (133, 88, 13).

6 Conclusions

We hope that this review has served as an (all too brief!) introduction to *some* of the exciting physics potentially accessible at a 500 GeV – 1 TeV linear electron positron collider. The technology now exists to build a machine of the required energy and luminosity to explore *with high precision* the energy range pertinent to the electroweak theory. It has been argued that the high precision measurements play a role both orthogonal to the measurements the LHC will make *and* supportive of some of the physics LHC will possibly see. For this reason a linear collider should be operational before the end of LHC running. Precision measurements at the TeV electroweak scale have been shown to be a potential window on much higher energy scales (even the Planck scale) in a large class of theories.

Within the electroweak theory, an electron-positron collider has been shown to have the capability to pin down quantum numbers and explore the chiral nature of couplings by virtue of the superior energy resolution and polarized beams. Options for collisions of electrons or photons have been described which shed even more light on the nature of couplings and can enhance signals over backgrounds. Specific examples have been given of the power a linear collider has to study the Higgs sector and identify particles and measure parameters in supersymmetric models.

Only a sampling of the alternative models have been described. Some of these theories could account for the large energy gap between the Planck and electroweak scales. Others provide possible explanations for the cosmological dark matter or dark energy. While we cannot predict exactly what new physics will emerge from the measurements at the TeV scale, we know from virtual effects in recent measurements that this energy scale will be active and lead to better understanding of the electroweak theory ... and possibly beyond. We argue that the high energy reach, particle production, precision and polarization of a combined LHC and e^+e^- collider program will be necessary to fully explore this physics.

7 Acknowledgements

MO is supported in part by the National Science Foundation under award nsf-phy/0201792. SD is supported by the Department of Energy, Contract DE-AC02-76CH00016. The authors thank the following for their generous assistance in preparing this article: Uli Baur, Jim Brau, Sean Carroll, Joe Lykken, Michael Peskin, Chris Quigg, David Rainwater, Tor Raubenheimer, Geraldine Servant, Savdeep Sethi, Mark Trodden, Michael Woods.

8 Bibliography

Literature Cited

1. Weinberg S. *Phys. Rev. Lett.* 19:1264 (1967); Salam A. In *Elementary Particle Theory*. Stockholm: Almquist and Wiksells (1969); Glashow SL, Iliopoulos J, Maiani L. *Phys. Rev. D* 2:1285 (1970)

2. 't Hooft G. In *Recent Developments in Gauge Theories*, ed G. 't Hooft, et al., p. 135. New York:Plenum (1980); Witten E. *Nucl. Phys. B* 188:513 (1981); Susskind L. *Phys. Rep.* 104:1 (1984)
3. Peskin M, Takeuchi T. *Phys. Rev. Lett.* 65:964 (1990); *Phys. Rev. D* 46:381 (1992)
4. LEP and SLD Collaborations. hep-ex/0312023
5. LEP Electroweak Working Group website. <http://www.cern.ch/LEPEWWG>
6. LEP Collaborations, *Phys. Lett.* **B565**, 61 (2003), hep-ex/0306033
7. Lee B, Quigg C, Thacker H. *Phys. Rev. D* 16:1519 (1977)
8. Branson J, et al. (ATLAS and CMS Collabs.). *Eur. Phys. J. direct C* 4:N1 (2002); Baur U, et al. *Proc. Snowmass Study on the Future of Particle Physics*, Snowmass, Colorado, 30 June-21 July 2001, (2001), hep-ph/0201227
9. ATLAS Collaboration. ATLAS Physics Technical Design Report, <http://atlas.web.cern.ch/Atlas/GROUPS/PHYSICS/TDR/TDR>. CMS Collaboration. CERN-LHCC-94-38 (1994)
10. High Energy Physics Advisory Panel. DOE/SC-0027 (2000); U.S. Department of Energy. "High Energy Physics Facilities Recommended for the Department of Energy Office of Science Twenty-year Roadmap" (2003) (http://doe-hep.hep.net/HEPFacSub/HEPAP_FacilitiesMar03.pdf)
11. Peskin M, Murayama H. *Ann. Rev. Nucl. Part. Sci.* 46:533 (1996), hep-ex/9606003
12. Accomando E, et al. *Phys. Rept.* 299:1 (1998), hep-ph/9705442
13. Ellis J. hep-ex/0210052
14. Grannis P, ed., *Understanding Matter, Energy, Space and Time: The Case for the Linear Collider*, http://sbhep1.physics.sunysb.edu/~grannis/ilcsc/lc_consensus.pdf; ALCWG, FERMILAB-PUB-00/152 (2000)
15. The American Linear Collider Working Group, *Linear Collider Physics Resource Book for Snowmass 2001*, May 2001, BNL-52627, CLNS 01/1729, FERMILAB-Pub-01/058-E, LBNL-47813, SLAC-R-570, UCRL-ID-143810-DR (<http://www.slac.stanford.edu/grp/th/LCBook>). Updates and additions to this document in the Snowmass 2001 eProceedings, <http://www.slac.stanford.edu/econf/C010630/proceedings.shtml>
16. *TESLA Technical Design Report*, March 2001, DESY 2001-11 (<http://www.desy.de/~lcnotes/tdr>)
17. ACFA Linear Collider Working Group. *ACFA Linear Collider Working Group Report*, November 2001, KEK-Report 2001-11, hep-ph/0109166
18. Bagger J, et al. hep-ex/0007022
19. Simmons E. hep-ph/0011244
20. Hill C, Simmons E. *Phys. Rept.* 381:235 (2003), hep-ph/0203079
21. Arkani-Hamed N, Cohen AG, Georgi H. *Phys. Lett. B* 513:232 (2001), hep-ph/0105239; Arkani-Hamed N, Cohen AG, Katz E, Nelson A. *JHEP* 07:034 (2002), hep-ph/0206021; Arkani-Hamed N, Cohen AG, Gregoire T, Wacker JG. *JHEP* 08:020 (2002), hep-ph/0202089
22. Csaki C, Grojean C, Murayama H, Pilo L, Terning J. hep-ph/0305237; Hall LJ, Nomura Y. *Phys. Rev. D* 64:055003 (2001), hep-ph/0103125; Davoudiasl H, Hewett J, Rizzo T. hep-ph/0312193
23. Trodden M, Carroll S. In *Proc. Theoretical Advanced Study Institute in Elementary Theory*, Boulder, Colorado, 1-27 June 2003, astro-ph/0401547
24. Baer H, Balazs C, Belyaev A, O'Farrill J. *JCAP* 0309:007 (2003), hep-ph/0305191; Ellis J, Feng J, Ferstl A, Olive K. *Eur. Phys. J. C* 24:311 (2002), astro-ph/0110225; Feng J, Matchev K, Wilczek F. *Phys. Rev. D* 63:045024 (2001), astro-ph/0008115
25. Ellis J, Olive K, Santoso Y, Spanos VC. *Phys. Lett. B* 565:176 (2003), hep-ph/0303043
26. Hewett J, Spiropulu M. *Ann. Rev. Nucl. Part. Sci* 52:396 (2002), hep-ph/0205106

27. Weiglein G. LHC/LC Study group report, <http://www.ipp.dur.ac.uk/georg/lhclc/>
28. Desch K, Kalinowski J, Moortgat-Pick G, Nojiri M, Polesello G. hep-ph/0312069
29. Oreglia M. ed. *Design Considerations for an International Linear Collider*, <http://blueox.uoregon.edu/~lc/scope.ps> (2003)
30. Heuer R. ed. *Parameters for the Linear Collider*, http://www.fnal.gov/directorate/icfa/LC_parameters.pdf (2003)
31. Battaglia M. In *Proc. 10th International Conference on Supersymmetry and Unification of Fundamental Interactions*, Hamburg, Germany, June 17-23 2002, hep-ph/0211461
32. Desch K. *Proc. 4th ECFA/DESY Workshop on Physics and Detectors for a 90 GeV to 800 GeV Linear e^+e^- Collider*, Amsterdam, The Netherlands, 1-4 Apr. 2003, hep-ph/0311092
33. Battaglia M, Desch K. *Proc. 5th International Linear Collider Workshop*, Batavia, Ill., 24-28 Oct. 2000, hep-ph/0101165
34. Gunion J, Haber H, Van Kooten R. In *Linear Collider Physics in the New Millennium*, ed. K. Fujii, et al., Singapore: World Scientific, hep-ph/0301023
35. Behnke T, Wells J, Zerwas P. *Prog. Part. Nucl. Phys.* 48:363 (2002)
36. Battaglia M, De Roeck A. *Proc. Snowmass Study on the Future of Particle Physics*, Snowmass, Colorado, 30 June-21 July (2001), hep-ph/0111307
37. Erler J, et al. *Proc. Snowmass Study on the Future of Particle Physics*, Snowmass, Colorado, 30 June-21 July (2001), hep-ph/0112070
38. Edwards DA, Syphers MJ. *An introduction to the Physics of High Energy Accelerators* Chicago:Wiley (1993); Chao AW, Tigner M. *Handbook of Accelerator Physics and Engineering*, Singapore:World Scientific (1999)
39. Heuer R. *Int. Jour. Mod. Phys. A* 17:3469 (2002), hep-ex/0111070
40. Phinney N, et al. (NLC Collab.). SLAC-R-571 (2001)
41. JLC Collab, KEK report 97-1, <http://acfahep.kek.jp/acfareport/index.html>
42. Guignard G, et al. (CLIC Study Team). CERN 2000-008 (2000)
43. Loew G, et al. (International LC Technical Review Committee) <http://www.slac.stanford.edu/xorg/ilc-trc/ilc-trchome.html>
44. International Linear Collider Steering Committee website: http://www.fnal.gov/directorate/icfa/International_ILCSC.html
45. Chen P. *Phys. Rev. D* 46:1186 (1992); Schulte D. eConf C980914:127 (1998)
46. Cinabro D, Torrence E, Woods M. *Status of LC Beam Instrumentation Design*, ALCPG Note LCD-ALCPG-03-0001 (2003), <http://www.slac.stanford.edu/xorg/lcd/ipbi/notes/white.pdf>; Frary MN, Miller DJ. In *Munich/Annecy/Hamburg 1991, Proceedings, e^+e^- collisions at 500-GeV, part A, 379-391 (1981); Boogert ST, Miller DJ. To appear in the proceedings of International Workshop on Linear Colliders (LCWS 2002), Jeju Island, Korea, 26-30 Aug 2002, hep-ex/0211021;
47. Woods M. *Int. J. Mod. Phys. A* 15:2529 (2000), hep-ex/0004004
48. Barger V, Beacom JF, Cheung K, and Han T, *Phys. Rev. D* 50:6704 (1994), hep-ph/9404335
49. Feng J, Peskin M. *Phys. Rev. D* 64:115002 (2001), hep-ph/0105100
50. Blochinger C, Fraas H, Moortgat-Pick G, Porod W. hep-ph/0201282
51. Freitas A, von Manteuffel A, Zerwas P. hep-ph/0310182
52. Gunion J. *Int. J. Mod. Phys. A* 18:2739 (2003); Asner D, et al. hep-ph/0308103
53. Rowson PC, Woods M. hep-ex/0012055
54. Erler J, Heinemeyer S, Hollik W, Weiglein G, Zerwas P. *Phys. Lett. B* 486:125 (2000), hep-ph/0005024; Baur U,

- et al. *Proc. Snowmass Study on the Future of Particle Physics*, Snowmass, Colorado, 30 June-21 July 2001, hep-ph/0202001
55. Schumm BA, talk presented at the 2001 Snowmass Workshop on the Future of Particle Physics (2001), hep-ex/0111009.
 56. Battaglia M, Hinchliffe I, Jaros J, and Wells J, *ibid.*, hep-ex/0201018
 57. TESLA Collaboration, in Part IV of the TESLA Technical Design Report, DESY/2001-011 (2001)
 58. Brau JE. In *Proc. Extended Joint ECFA/DESY Study on Physics and Detectors for a Linear Electron-Positron Collider*, ed. R. Settles (2003), <http://www.desy.de/conferences/ecfa-desy-lcext.html>
 59. Briant JC, Videau H, hep-ex/0202004
 60. Brau JE, In *Proc. of the International Workshop on Linear Colliders 2002*, p. 675, ed. J.S. Kang and S.K. Oh, Korean Physical Society (2003)
 61. Zeppenfeld D. *Proc. Snowmass Study on the Future of Particle Physics*, Snowmass, Colorado, 30 June-21 July 2001, hep-ph/0203123; M. Duerhson. ATLAS Physics Note (2003)
 62. Choudhury D, Tait T, Wagner, CEM. *Phys. Rev. D* 65:115007 (2002), hep-ph/0202162
 63. Kniehl BA. hep-ph/0210175; Dittmaier S. hep-ph/0308079
 64. Potter C, Brau J, Iwasaki M. *Proc. Snowmass Study on the Future of Particle Physics*, Snowmass, Colorado, 30 June-21 July (2001)
 65. Kuhl J. <http://www-flc.desy.de/ecfa-higgs/montpellier/kuhl-montpellier.pdf>
 66. Juste A, Merino G. hep-ph/9910301; Gay A. ECFA/DESY Workshop; Baer H, Dawson S, Reina L. *Phys. Rev. D* 61:013002 (2000), hep-ph/9906419
 67. Baur U, Plehn T, Rainwater D. *Phys. Rev. D* 68:033001 (2003), hep-ph/0304015; Castanier C, Gay P, Lutz P, Orloff J. hep-ph/0101028; Battaglia M, Boos E, Yao WM. hep-ph/0111276
 68. Djouadi A, Kilian W, Mühlleitner MM, Zerwas P. *Eur. Phys. J. C* 10:27 (1999), hep-ph/9903229
 69. Miller DJ, Choi SY, Eberle B, Mühlleitner MM, Zerwas P. *Phys. Lett. B* 505:149 (2001), hep-ph/0102023
 70. Dova MT, Garcia-Abia P, Lohmann W. hep-ph/0302113
 71. Choi SY, Miller DJ, Mühlleitner MM, Zerwas P. *Phys. Lett. B* 553:61 (2003), hep-ph/0210077; *Phys. Rev. D* 49:79 (1994), hep-ph/9306270
 72. Degrassi G, Heinemeyer S, Hollik W, Slavich P, Weiglein G. *Eur. Phys. J. C* 28:133 (2003), hep-ph/0212020
 73. Quiros M, Espinosa J. In *Particles, Strings, and Cosmology*, Boston (1998), hep-ph/9809269; Kane G, Kolda C, Wells J. *Phys. Rev. Lett.* 70:2686 (1993), hep-ph/9210242.
 74. Guasch J, Hollik W, Penaranda S. hep-ph/0307012; *Phys. Lett. B* 515:367 (2001), hep-ph/0106027
 75. Battaglia M, Desch K. hep-ph/0102265
 76. Moretti S. hep-ph/0306297; hep-ph/0209210; Logan H, Su SF. *Phys. Rev. D* 66:035001 (2002), hep-ph/0203270
 77. Martin SP. *A Supersymmetric Primer*, In *Perspectives on Supersymmetry*, ed. G. Kane Singapore: World Scientific (1997), hep-ph/9709356; Chung D, Everett L, Kane G, King S, Lykken J. hep-ph/0312378; Dawson S. *Proc. Theoretical Advanced Study Institute in Elementary Particles*, Boulder, Colorado, June 1997, hep-ph/9712464; Polonsky N. *Lecture Notes in Physics Monographs*, Vol. m68. Heidelberg: Springer-Verlag (2001), hep-ph/0108236
 78. Feng J, Nojiri M. hep-ph/0210390
 79. Danielson MN, et al. *Proc. Snowmass Study on the Future of Particle Physics*, Snowmass, Colorado, 30 June-21 July 2001
 80. Drees M. *Lectures given at the Inauguration Conference of the Asia Pacific Center for Theoretical Physics*, Seoul, Korea, 4-19 June 1996, hep-ph/9611409
 81. Bachacou H, Hinchliffe I, Paige F. *Phys. Rev. D* 62:015009 (2000), hep-ph/9907518

82. Battaglia M, et al., *Proc. Snowmass Study on the Future of Particle Physics*, Snowmass, Colorado, 30 June-21 July 2001, hep-ph/0201177
83. Dreiner H. *An Introduction to Explicit R Parity Violation, Perspectives on Supersymmetry*, ed. G. Kane Singapore: World Scientific (1997), hep-ph/9707435
84. Feng J, Peskin M, Murayama H, Tata X. *Phys. Rev. D* 52:1418 (1995), hep-ph/9502260
85. Martyn H, Blair G. hep-ph/9910416
86. Chamseddine A, Arnowitt R, Nath P. *Phys. Rev. Lett.* 49:970 (1982); Barbieri R, Ferrara S, Savoy C. *Phys. Lett. B* 119:343 (1982); Hall L, Lykken J, Weinberg S. *Phys. Rev. D* 27:2359 (1983)
87. Djouadi A, Drees M, Kneur J. *JHEP* 0108:055 (2001), hep-ph/0107316
88. Baer H, Belyaev A, Krupovnickas T, Tata X. hep-ph/0311351
89. Dine M, Fischler W. *Nucl. Phys. B* 204:346 (1982); Dimopoulos S, Raby S. *Nucl. Phys. B* 219:479 (1983); Dine M, Nelson A. *Phys. Rev. D* 48:1277 (1993), hep-ph/9303230; Dine M, Nelson A, Shirman Y. *Phys. Rev. D* 51:1362 (1995)
90. Blair G, Porod W, Zerwas P. *Phys. Rev. D* 63:017703 (2001), hep-ph/0007107; *Eur. Phys. J. C* 27:263 (2003), hep-ph/0210058
91. Bagger J, Falk A, Schwartz M. *Phys. Rev. Lett.* 84:1385 (2000), hep-ph/9908327; Chivukula RS, Hoelbling C, Evans N. *Phys. Rev. Lett.* 85:511 (2000), hep-ph/0002022; Alam S, Dawson S, Szalapski R. *Phys. Rev. D* 57:1557 (1998), hep-ph/9706542; Barbieri R, Strumia A *Phys. Lett. B* 462:144 (1999), hep-ph/9905281; Kolda C, Murayama H. *JHEP* 00007:035 (2000), hep-ph/0003170
92. Barklow T, Chivukula RS, Goldstein J, Han T. *Proc. Snowmass Study on the Future of Particle Physics*, Snowmass, Colorado, 30 June-21 July 2001, hep-ph/0201243
93. Peskin M, Wells J. *Phys. Rev. D* 64:093003 (2001), hep-ph/0101342
94. Fujii K, Matsui T, Sumino Y. *Phys. Rev. D* 50:4341 (1994)
95. Martinez M, Miquel R. *Eur. Phys. Jour. C* 27:49 (2003), hep-ph/0207315
96. Hoang AH, hep-ph/0307376
97. Hoang AH, Teubner T. *Phys. Rev. D* 60:114027 (1999), hep-ph/9904468; Hoang AH, Ligeti Z, Manohar AV. *Phys. Rev. Lett.* 82:277 (1999), hep-ph/9809423
98. Hoang AH, Stewart IW. *Phys. Rev. D* 67:114020 (2003), hep-ph/0209340
99. Arkani-Hamed N, Dimopoulos S, Dvali G. *Phys. Lett. B* 429:263 (1998), hep-ph/9803315
100. Antoniadis I, Benakli K. *Int. J. Mod. Phys. A* 15:4237 (2000), hep-ph/0007226
101. Davoudiasl H. *Phys. Rev. D* 61:044018 (2000), hep-ph/9907347; Ghosh DK, Raychaudhuri S. *Phys. Lett. B* 495:114 (2000), hep-ph/0007354; Choudhury SR, Cornell AS, Joshi GC. *Phys. Rev. D* 64:114022 (2001), hep-ph/0105002; *Phys. Lett. B* 535:289 (2002), hep-ph/0202272; Ghosh DK, Mathews P, Poulouse P, Sridhar K. *JHEP* 9911:004 (1999), hep-ph/9909567
102. Rizzo T. *JHEP* 0302:008 (2003), hep-ph/0211374
103. Èboli OJ, Magro MB, Mathews P, Mercadante PG. *Phys. Rev. D* 64:035005 (2001), hep-ph/0103053
104. Giudice GF, Rattazzi R, Wells J. *Nucl. Phys. B* 544:3 (1999), hep-ph/9811291
105. Han T, Lykken J, Zhang RJ. *Phys. Rev. D* 59:105006 (1999), hep-ph/9811350
106. Cheung K, Landsberg G. *Phys. Rev. D* 65:076003 (2002), hep-ph/0110346
107. Agashe K, Deshpande NG. *Phys. Lett. B* 456:60 (1999), hep-ph/9902263
108. Hewett J, Petriello FJ, Rizzo T. *Phys. Rev. D* 64:075012 (2001), hep-ph/0010354
109. Mirabelli EA, Perelstein M, Peskin M. *Phys. Rev. Lett.* 82:2236 (1999), hep-ph/9811337
110. Gopalakrishna S, Perelstein M, Wells J. hep-ph/0110339

111. Dutta S, Konar P, Mukhopadhyaya B, Raychaudhuri S. *Phys. Rev. D* 68:095005 (2003), hep-ph/0307117
112. Randall L, Sundrum R. *Phys. Rev. Lett.* 83:4690 (1999), hep-th/9906064; *Phys. Rev. Lett.* 83:3370 (1999), hep-ph/9905221
113. Davoudiasl H, Hewett J, Rizzo T. *Phys. Rev. D* 63:075004 (2001), hep-ph/0006041
114. Rai SK, Raychaudhuri S. *JHEP* 0310:020 (2003), hep-ph/0307096
115. Hewett J, Rizzo T. *JHEP* 0308:028 (2003), [hep-ph/0202155].
116. Appelquist T, Cheng HC, Dobrescu B. *Phys. Rev. D* 64:035002 (2001), hep-ph/0012100
117. Carone CD, Conroy JM, Sher M, Turan I. hep-ph/0312055
118. Lindner EV, ed. *Resource Book on Dark Energy*, compilation from Snowmass 2001, <http://supernova.lbl.gov/~evlinder/sci.html>
119. <http://background.uchicago.edu/~whu/physics/physics.html>
120. Perlmutter S, et al. (Supernova Cosmology Project Collab.). *Astrophys. Journ.* 517:565 (1999), astro-ph/9812133
121. Bennett CL, et al. *Astrophys. J. Suppl.* 148:1 (2003), astro-ph/0302207
122. Spergel DN, et al. *Astrophys. J. Suppl.* 148:175 (2003), astro-ph/0302209
123. Chattopadhyay U, Corsetti A, Nath P. *Phys. Rev. D* 68:035005 (2003), hep-ph/0303201
124. Verde L. *New Astronomy Reviews* 47:713 (2003)
125. Jungman G, Kamionkowski M, Griest K. *Phys. Rept.* 267:195 (1996), hep-ph/9506380
126. Feng J. hep-ph/0012277
127. Cheung HY. *Phys. Rept.* 158:1 (1988); Kim JE. *Phys. Rept.* 150:1 (1987)
128. Servant G, Tait T. *Nucl. Phys. B* 650:391 (2003), hep-ph/0206071
129. Cembranos JA, Dobado A, Maroto AL. *Phys. Rev. Lett.* 90:241301 (2003), hep-ph/0302041
130. Cheng HC, Feng J, Matchev KT. *Phys. Rev. Lett.* 89:211301 (2002), hep-ph/0207125
131. Ellis J, Falk T, Ganis G, Olive K. *Phys. Rev. D* 62:075010 (2000), hep-ph/0004169
132. Birkedahl-Hansen A. private communication
133. Richard F. *Proc. 21st International Symposium on Lepton and Photon Interactions at High Energies*, Batavia, Ill., 11-16 Aug. 2003, hep-ph/0312020
134. Sakharov AD. *Zh. Eksp. Teor. Fiz. Pis'ma* 5:32 (1967); *JETP Lett. B* 91:24 (1967)
135. Langacker P. *Phys. Rept.* 72:185 (1981)
136. Trodden M. hep-ph/0302151, Zlatev I, Wang L, Steinhardt P. *Phys. Rev. Lett.* 82:896 (1999), astro-ph/9807002
137. Carena M, Quiros M, Seco M, Wagner CEM, *Nucl. Phys. B* 650:24 (2003), hep-ph/0208043
138. Procopec T et al. hep-ph/0302192
139. Mohapatra RN, Senjanovic G. *Phys. Rev. D* 12:1502 (1975); Fukugita M, Yanagida T. *Phys. Lett.* 174:45 (1986); Gell-Mann M, Ramond P, Slansky R. In *Supergravity*, ed. P. Van Nieuwenhuizen and D.Z. Freedman, North Holland (1979); Langacker P, Peccei RD, Yanagida T, *Mod. Phys. Lett. A* 1:541 (1986); Luty M. *Phys. Rev. D* 45:455 (1992)
140. Affleck I, Dine M. *Nucl. Phys. B* 249:361 (1985)